KFKI-1982-31

L.P. CSERNAI
H. STÖCKER
P.R. SUBRAMANIAN
G. BUCHWALD
G. GRAEBNER
A. ROSENHAUER
J.A. MARUHN
W. GREINER

FRAGMENT EMISSION IN RELATIVISTIC HEAVY-ION REACTIONS

Hungarian Academy of Sciences

CENTRAL
RESEARCH
INSTITUTE FOR
PHYSICS

BUDAPEST

2017

KFKI-1982-31

FRAGMENT EMISSION IN RELATIVISTIC HEAVY-ION REACTIONS

LÁSZLÓ P. CSERNAI

Institut für Theoretische Physik
Johann Wolfgang Goethe Universität
D-6000 Frankfurt am Main 1, West Germany and
Central Research Institute for Physics
H-1525 Budapest 114, P.O.B. 49, Hungary

HORST STÖCKER

Gesellschaft für Schwerionenforschung
D-6100 Darmstadt, West Germany

PAL R. SUBRAMANIAN[+], GERD BUCHWALD, GERHARD GRAEBNER,
ALBRECHT ROSENHAUER, JOACHIM A. MARUHN, and WALTER GREINER

Institut für Theoretische Physik
Johann Wolfgang Goethe Universität
D-6000 Frankfurt am Main 1, West Germany

Submitted to Physical Review C

HU ISSN 0368 5330
ISBN 963 371 917 8

[+]Present address: University of Madras, India

ABSTRACT

We present a theoretical description of nuclear collisions which consists of a three-dimensional fluid-dynamical model, a chemical equilibrium break-up calculation for local light fragment (i.e. p, n, d, t, ^{3}He, ^{4}He) production and a final thermal evaporation of these particles. The light fragment cross section and some properties of the heavy target residues are calculated for the asymmetric systems Ne + U at 400 MeV/N, Ne + Pb at 800 MeV/N and C + Sn at 86 MeV/N. The results of the model calculations are compared with recent experimental data. Several observable signatures of the collective hydrodynamical processes are consistent with the present data. An event-by-event analysis of the flow patterns of the various clusters is proposed which can yield deeper insight into the collision dynamics.

АННОТАЦИЯ

Сечение легких ядер и остатков пышени вычисляется в гидродинамическо - эвапорационном модели релятивстических реакций тяжелых ионов и результат сравнивается с экспериментом.

KIVONAT

Bemutatjuk atommagütközések egy elméleti leirását, amely egy 3-dimenziós folyadék dinamikai modellt, egy a könnyü atomi fragmentek (p, d, t, ^{3}He, ^{4}He) közti kémiai egyensulyt feltételező feltörési számitást és ezen részecskék végső termikus elpárolgását irja le. A könnyü mag hatáskeresztmetszetek és a nehéz target maradványok néhány tulajdonságát a Ne + U (400 MeV/n), a Ne + Pb (800 MeV/n) és a C + Pb (86 MeV/n) aszimmetrikus rendszerekre kiszámitottuk, és összehasonlitottuk kisérleti adatokkal. A kollektiv hidrodinamikai folyamatok számos észlelhető jele összevág a jelenlegi kisérleti adatokkal. A fragmentek áramlásának egy eseményenkénti analizisét javasoljuk, amely a reakció-dinamikába mélyebb betekintést nyujthat.

1. Introduction

Recent experimental results [1-5] on fragment emmission in high energy nuclear collisions can be qualitatively understood as being due to collective flow processes as predicted by the hydrodynamic model [1,5-18] In this paper we will present a quantitative comparison of the main experimental results with an extended fluid dynamical model, which also includes a calculation of the light cluster production and their spectra.

The various models constructed so far to describe high energy heavy ion reactions rely on basically different assumptions: In the fireball model [19] a global thermal equilibration is assumed among all participant nucleons . In the firestreak model [20] this requirement is relaxed to smaller partitions, (streaks) while in the hydrodynamic model only local equilibrium is required. On the other hand the cascade models assume no equilibrium and in their different existing versions different types of equilibration are reached during the collision. The extent of equilibration depends essentially on the mean free path λ of the nucleons. The mean free path of an impinging proton in the nucleus has recently been determined experimentally to be λ=2.4fm.[21] However, owing to the increasing temperature and density this value can become much smaller in nucleus-nucleus collisions. First experimental results [22] yielded λ=1 fm. Hence local equilibrium may be achievable and hydrodynamic effects may become important, in particular if heavier systems are investigated. Experimentally the equilibration may be studied by the comparision of the light fragment spectra.[23]

There is a considerable amount of theoretical studies of fragment production. Many of these assume that a fireball is produced, which can be characterized by global thermal and chemical equilibrium. They differ from each other in the statistics applied (ideal classical,[24-26] quantum,[20,27-29] quantum with interactions [30,31]) and in the number of the considered composite fragments which is usually small, but can go above one hundred by considering all stable and excited states of nuclei up to A=16.[24] In these models the thermal energy is identical to the initial total CM kinetic energy. This extreme assumption is mitigated by the consideration of the possible collective flow (or expansion) which may carry a large fraction of the available energy.[6,25,32-34] In these models, some effects of the expansion or explosion have been studied in simplified spherical geometry, as e.g.in the blast-wave model [35] and in the different versions of the hadron chemistry model.[36] Already in the case of the simple

spherical expansion the inclusion of viscous effects into the relativistic hydrodynamic description [6] can have a strong effect on the observable fragment ratios, as was pointed out recently.[33] Unfortunately the simple spherical geometry assumed in these models is not very realistic.

In the present calculation we combine the viscous hydrodynamical model (Sect. II) for the collision process with a chemical equilibrium break - up model and a final thermal evaporation calculation (Sect. III) to obtain the spectra of the light particles. In Sect. IV we present the results for mean values and fluctuations of the light fragment multiplicities. Sect. V contains our results on the double and triple differential cross sections of the light fragments and an analysis of the particle correlations. The formation of heavy fragments and some of their properties are discussed in Sect. VI. An event-by-event analysis for the different fragments is performed in Sect. VII. The conclusions are given in the last section.

II. The hydrodynamic model

If we derive the hydrodynamic equations from the Boltzmann transport theory we assume that the system can be characterised by thermally equilibrated local momentum distributions or by distributions close to the equilibrated ones. In the former case we obtain the Euler equations of hydrodynamics, and in the latter the Navier-Stokes equations, which also include a description of the transport properties of the fluid. If the local momentum distributions are far from the equilibrium ones, a two-[37] or multi- fluid[38] description may be applied. The classical equations of hydrodynamics can be formulated as conservation equations for mass, momentum, and energy. The local baryon density $n(r,t)$ and the flow velocity field $v(r,t)$ obey the continuity equation

$$\partial n/\partial t + \mathrm{div}(nv) = 0 \,. \tag{1}$$

The conservation of momentum density, $M = \rho v = n m_N v$ is given by

$$\partial(M)/\partial t + \mathrm{Div}(M \bullet v) = \mathrm{Div}\, P - n\, \mathrm{grad}(V), \tag{2}$$

where $M \bullet v$ denotes the dyadic product and P is the stress tensor given by

$$P_{ij} = -p\delta_{ij} + \eta[\partial v_i/\partial x_j + \partial v_j/\partial x_i - (2/3)\delta_{ij}\,\mathrm{div}(v)\,] + \zeta\,\delta_{ij}\,\mathrm{div}(v). \tag{3}$$

Here the scalar pressure p is given by the equation of state and the viscous stress tensor involvs the shear viscosity $\eta(\rho,T)$ and the bulk viscosity $\zeta(\rho,T)$. The interaction potentials V are not included in the nuclear matter equation of state because of their long-range properties. Accordingly V is defined as a sum of a Yukawa and a Coulomb contribution, V_Y and V_C. (The way these potentials are determined and the choice of their parameters are described in Ref. 7.) The equation for conservation of energy takes the form

$$\partial(nE)/\partial t + \mathrm{div}(nEv) = \mathrm{div}(Pv) - \mathrm{div}(-\kappa\,\mathrm{grad}(T)) - nv\,\mathrm{grad}(V) \tag{4}$$

where κ is the coefficient of thermoconductivity and E is the energy per baryon (including kinetic and internal energy). In the actual calculations fixed parameters η= 10-20 MeV/fm^{2}c ζ=0, and κ=0 were used.

To complete the set of equations of motion in the hydrodynamic model, an equation of state has to be specified. This is usually done by giving the binding energy per nucleon at zero entropy as a function of the density, $W_o = W_o(n)$. For finite entropy per nucleon s, the corresponding excitation energy of an ideal Fermi gas is added:

$$W(n,s) = W_o(n) + W_T(n,s). \tag{5}$$

All other thermodynamic quantities may be obtained easily from W(n,s):

$$T = (\partial W/\partial s)_n\ ,\ p = n^2(\partial W/\partial n)_s. \tag{6}$$

The binding energy per nucleon at zero entropy, $W_o(n)$ is called the compressional energy. One possible form of this function that was employed in most of the calculations uses a parabolic expansion about nuclear matter equilibrium :

$$W_o(n) = K_o(n-n_o)^2/(18n\ n_o) + B_o \qquad (7)$$

with K_o, the incompressibility of nuclear matter, usually set equal to 200 MeV, B_o to -16 MeV, and n_o equal to 0.17 fm^{-3}.

Numerical solutions were performed on a grid of cell size $\Delta x = 1 - 1.2$ fm. This relatively rough grid just enabled us to decrease the numerical viscosity[39] to the value of the used physical one. A detailed analysis of the effects of the equation of state and transport parameters is not the subject of the present work.[13] We estimate the uncertainties arising from numerical reasons to be less than 10 - 20 %. The total conservation laws (for mass, momentum, energy) are fulfilled, however, within a 5 % accuracy.

Solving the equations of motion of fluid dynamics in the realistic three-dimensional geometry of a nuclear collision is a very expensive computation. As long as the collision of the two nuclei is supersonic, that is their relative velocity is greater than 0.1-0.2c, shock waves [40] will be the dominant dissipation mechanism in the hydrodynamic model. Due to the large pressure that builds up in the shocked interaction zone, hydrodynamic models show a prefered sideward emission in central collisions. Such predictions, as we will see later, find a support by the emission patterns of α - particles and protons that have been observed in high multiplicity selected events of particle track detector [1] and counter data [2-4] respectively.

Collisions very close to central do not contribute much to the cross section, so that for measurability considerations it is imperative to examine the behaviour at larger, especially intermediate impact parameters. At intermediate impact parameters a different phenomenon is predicted in the hydrodynamic model, namely the "bounce - off" effect [14] where the projectile matter as a whole essentially is deflected by the target collectively (Fig. 1).

III. Chemical equilibrium at break-up - Light fragment production

To draw accurate quantitative conclusions regarding the experimental observables in the final state an evaporation model is attached to the

hydrodynamic calculations,[5,6,13,15-17,41,42] because at late expansion stages of the collision process when the matter is already dilute the conditions of the hydrodynamic description are not fulfilled. The pressure gradually decreases and a transition from nuclear matter to separate nuclei takes place like e.g., the surface phase transition in the neutron stars.[43] Here this gradual transition is even more complicated, because we are in a dynamic system and during the transition the interactions also cease. Small fragments condensate out of nuclear matter, forming light nuclei. These then loose their contact owing to the further expansion of the system.

In the model this gradual transition is replaced by a sudden break-up process. The break-up moment is chosen for all impact parameters to be that moment when the maximum nucleon density in the matter is below normal nuclear density. So the average density at break-up is $\rho = 0.05 - 0.07/fm^3$. Unfortunately the continuous break-up in time, which is used in simple linear and spherical fluid dynamical models [6,41,42] would cause tremendous difficulties in general three-dimensional case, so that we had to choose the sudden break-up assumption as in previous calculations in the hydrodynamic and evaporation model.[5,13,15,17] Based on Refs. 36 and 41 we assume that at the break-up moment the chemical and thermodynamical equilibrium is already established locally among the light nuclear fragments. Thus the densities of different nuclei (i = p,n,d,t,^{3}He,^{4}He) are determined by statistical factors:[24-27]

$$n_i(n_p,n_n,T) = a_i\, n_p^{Z_i}\, n_n^{N_i}\,, \tag{8}$$

where $a_i = \lambda_T^{3A_i-3}\, A_i^{3/2}\, 2^{-A_i} \exp(E_o^{(i)}/kT)\, \Sigma_j\, (2S_j+1) \exp(-E_j^{(i)}/kT)$, and $\lambda_T = h/\sqrt{2\pi m_p kT}$, is the thermal de Broglie wave length. The density of a given fragment i of charge Z_i and neutron number N_i ($A_i=N_i+Z_i$) depends on the common temperature T of the mixture, on the proton and neutron densities n_p, n_n and on the physical properties of the fragment i, namely on the ground state energy $E_o^{(i)}$, the excited state energies $E_j^{(i)}$ (measured from $E_o^{(i)}$) and spins S_j. The unknown parameters n_p, n_n, T can be obtained from the conservation of local baryon number, charge and energy:

$$
\begin{aligned}
n \quad &= A_{cell}/V_{cell} = \Sigma_i\, n_i\, A_i \,, \\
n\, Z/A &= Z_{cell}/V_{cell} = \Sigma_i\, n_i\, Z_i \,, \\
\varepsilon + n\, m_N &= E^{int.}_{cell}/V_{cell} + n\, m_N = \Sigma_i\, n_i (m_i + 3T/2) \,,
\end{aligned}
\tag{9}
$$

where n is the baryon density in the fluid cell at the break-up moment and $E^{int.}_{cell}$ the total internal energy of the fluid cell including binding ($k_{Boltz.}=1$). A solution of Eqs. (9) with positive temperature T exists only in those cells where the internal excitation energy is not too low. In the regions where $E^{int.} \ll 8$ MeV/nucleon light fragments cannot be formed (there is no physical solution for Eqs.(9)), but a larger nucleus can be created from the contribution of some neighboring fluid cells (see Sect. VI).

It has to be noted that this is not a unique choice of the conserved quantities. In Ref. 17 it is assumed that the entropy is constant during the break-up process. As was pointed out by Scott and Tripathi [44] the disasambly of nuclear matter represents a first-order phase transition below a critical temperature of $T_c \approx 18$-20 MeV and so an entropy increase may be obtained at the break-up. This shows up as an enhancement of the light fragment emission compared to naive fireball predictions. In our description we do not fix the entropy during break-up and we obtain an increase of the specific entropy of about 10-20% arising from the fragment formation at low temperatures. At higher temperatures where mainly free nucleons are formed the entropy hardly changes.

The ratios of the different light nuclear fragments are sensitive to the local temperature at break-up. Since, however, only a minor part of the entropy is produced in the expansion stage [6,13,41] even in viscous flows, the entropy produced in the compression shock-waves can be estimated relatively accurately. The specific entropy s after the break-up moment in each fluid cell can be estimated as:

$$
s = \Sigma_i [\, 5/2 + 3/2 \ln T + q_i - \ln n_i + \ln g_i]\, n_i/n \tag{10}
$$

where $q_i = c_v \ln(2\pi m_i/h^2)$ and g_i is the spin degeneracy factor.

In hydrodynamic calculations we can evaluate the local specific entropies before and after the break-up. The latter ones influence the observed

light particle cross sections together with the local collective flow. Once the influence of the collective flow in the final state has been extracted, the local thermal excitation of projectile and target can be determined from the ratios of the different light fragments in certain regions of the rapidity space.

In the following calculations as we shall see (Table I) a strong average entropy increase occurs at break-up. This increase has two reasons. The entropy determined after the break-up is the average specific entropy of those regions where light particles (p-^{4}He) are emitted. These are the hottest regions of the collision, where the entropy also is larger. The low entropy of the deeply bound fluid cells does not appear in the entropy of the light particles. On the other hand the formation of composite fragments leads to temperature and entropy increase in the hot regions also, because we gain the binding energies of the small fragments. These two effects lead to a smaller entropy decrease at low bombarding energies than it is expected on the basis of the Rankine-Hugoniot equation with some given equation of state. Other effects [31-33] also act in this direction so that a quantitative conclusion about the total entropy of the final state as given in Ref. 25 is hardly possible on the basis of the light fragment production ratios alone.

Recent studies of this evaporation process [27,30-32] show that the consideration of the interactions among the fragments causes strong deviations from the ideal gas assumption especially for the deuteron to proton ratio. If we increase the density of the deuteron nucleon gas mixture at fixed temperature, initially the deuteron density increases. But contrary to the ideal gas predictions at a certain density the deuteron to nucleon ratio reaches a maximum and the further density increase leads to a decrease of the d/n ratio. This can be taken into account by the explicit consideration of the eigenvolumina V_i of the fragments [27,32] for dilute gases. Generalizing the above mentioned approach [32] to our case a correction can be obtained to the a_i factor of Eq.(8):

$$a_i' = a_i \exp[\,-(V_i - N_i V_n - Z_i V_p)(n_i + n_n + n_p)\,] \approx a_i \exp[\,-(V_i - N_i V_n - Z_i V_p)\, n\,]. \tag{11}$$

Due to this factor the creation of fragments with large eigenvolumina (like d) is strongly suppressed especially at higher densities. The eigenvolumina V_i are taken from Ref. 45.

In Fig. 2 the local fragment densities $n_i(r)$ for p and α are shown after the break-up of the nuclear matter. In the central hot region mainly protons are formed while in the colder side regions (see Fig. 1) the heavier fragments are emitted preferentially.

Once the partial densities and the equilibrium temperature are given, the thermal momentum distributions in the fluid cell at r can be written as:

$$ {}^1_iF_H(P,r) = n_i(r)\ (2\pi m_i T(r))^{-3/2}\ \exp(-P^2/2m_iT(r)). \tag{12} $$

Since the fluid is moving with the local collective velocity $v(r)$, these distributions should be transformed to the lab system by a Lorentz transformation. The differential cross section of particle of type i

$$ d\sigma_i/dP \equiv {}^1\sigma_i(P) = \int d^2b\ d^3r\ {}^1_iF_H(P,r) \tag{13} $$

is obtained by adding up the contributions of all fluid cells in the lab system and then summing up the results of the different impact parameter calculations weighted by the corresponding geometrical surfaces.

In previous hydrodynamic model studies it turned out that the applicability of the model in the energy range discussed is restricted to the central and near central collisions of sufficiently massive nuclei.[5,42,46] In other words for peripferal collisions or for collisions of small nuclei like C + C the model, as a continuum model, is not appropriate. Here the relatively few collisions among the participant nucleons can be followed more accurately in a cascade model. Thus in the following part of the paper we discuss mainly "central" collisions. Within the hydrodynamic model it is not trivial to decide which impact parameters belong to a specific experimental trigger mode, because the fluctuations are not described by the model. We therefore use a cascade simulation of Toneev [47] where for the 393 MeV/N Ne + U collision the experimental high multiplicity selection ($M_{tot} > 10$) was studied and the contribution of the different impact parameter collisions were determined (Fig. 3). In most of the following applications we discuss the same reaction and take the given smooth cut-off function of Fig. 3 for the description of central collisions.

IV. Multiplicities and their fluctuations

First let us calculate the multiplicities of the various light particles from p to ^{4}He in the above model (Table I). From these quantities the total charged light particle multiplicities $N_{tot} = \Sigma_{i=p-^4He} N_i$ and the total bound proton multiplicities $N_{Bp} = \Sigma_{i=d-^4He} Z_i N_i$ can be obtained. These values are expectation values obtained under the assumption that the local momentum distributions are equivalent to that of an ideal gas mixture of light nuclear fragments. Even if we neglect the fluctuations arising from this assumption a lower bound for the fluctuations can be obtained in the following way. We have Z protons in our system and we expect that N_{Fp} free protons are produced in a collision with a given impact parameter and energy. The probability to find a given proton as a free one is

$$p = N_{Fp} / Z, \tag{14}$$

and the probability to find it in a cluster is

$$1 - p = (Z - N_{Fp}) / Z. \tag{15}$$

Therefore the probability to find n free protons is described by the following binomial distribution:

$$w(n) = p^n (1 - p)^{Z-n} \; Z! / [n! (Z - n)!], \tag{16}$$

and the expectation value of the fluctuation of the free proton number is ΔN_{Fp}

$$\langle \Delta N_{Fp}^2 \rangle = \langle n^2 \rangle - \langle n \rangle^2 = (1-p)\langle n \rangle = N_{Fp} (Z-N_{Fp}) / Z. \tag{17}$$

A second source of the fluctuations is the limited sensitivity range of the experimental devices, e.g. the Plastic Ball.[48] Assuming that the fluctuations arising from these two effects are independent the relative fluctuations can be added to each other

$$[\Delta N_{Fp}/N_{Fp}]^{obs.} = [\Delta N_{Fp}/N_{Fp}]^{thermodyn.} + [\Delta N_{Fp}/N_{Fp}]^{detector} . \quad (18)$$

Since after the collision Q free nucleons are produced and one nucleon is observed by the detector with a probability q the total observable fluctuation can be estimated as:

$$\Delta N_{Fp}^{obs.} = q\sqrt{(1-p)\ p\ Z} + \sqrt{(1-q)\ q\ p\ Z} , \quad (19)$$

where the first therm describes the thermal fluctuations and the second one the limited sensitivity of the detector. The calculated energy spectra provide us with a possibility to estimate roughly the detector sensitivity for a given reaction. Neglecting the limited angular range of the detector we take into account the lower energy cut only in these estimates. In Fig. 4 the *calculated* energy spectra $d\sigma_i/dE$ (i=p-^{4}He) of a central Ne + U → i + X reaction are plotted. The lowest particle energies which were considered in the preliminary Plastic Ball experiments when free and bound proton multiplicities were determined [48] are indicated for the light fragments. One can see that according to our calculations a non-negligible part of the composite particles is emitted below the considered energy cuts (the cross section scale is logarithmic and the lower energy cuts for p, d, t, ^{3}He and ^{4}He were taken as 34, 22, 19, 40, 34 MeV/N respectively). So the multiplicities above these energies are estimated to be 42, 56, 29, 12, and 5 % of the total ones in the Ne+U (393 MeV/N) reaction *according to our calculations.* For the Ne + Pb reaction at 800 MeV/N beam energy we estimated the acceptances as 80, 67, 42, 18 and 8 % respectively in the same way. At the higher beam energies the estimated acceptances increase and also other effects like final state Coulomb interaction may cause an increase in the acceptance. Due to the near exponential fall-off of the energy spectra, however, the measured multiplicities always depend strongly on the lowest energy considered. This dependence is less pronounce when the lower cut-off is choosen in the vicinity of the maximum of the energy spectra i.e. around 5-15 MeV/N. This might be possible with a more sophisticated analyses of the primary Plastic Ball data.[48]

In Fig. 5 the different reduced free and bound proton multiplicities are shown including the estimated sensitivity for the given reaction. The multiplicities decrease considerably and the fluctuations increase due to the reduction. For qualitative comparision preliminary experimental data are also

shown.[48] The multiplicities agree qualitatively, the experimental fluctuations are similar to our estimates and at large impact parameters there are more free and less bound protons observed than our model predicts. This is partly due to the fact that we neglected the impact parameter dependence of the acceptances and calculated always with the acceptance values corresponding to "central" collisions. So for peripferal collisions we overestimated the acceptance of the composite particles. The other reason can be seen from the detailed light particle multiplicities.

In Fig. 6 the different light particle multiplicities are plotted versus the total light particle multiplicity (only the reduced data, the original multiplicities are listed in Table I). In these light fragment multiplicities the tritons are overestimated compared to the recent experimental data of Gutbrod et al.,[48] while all others agree relatively well with the experiment. The triton excess is probably caused by the assumed large neutron excess of the evaporating nuclear matter (Z/A=0.447). The one fluid hydrodynamic model necessarily assumes a constant n_n/n_p ratio. In peripferal asymmetric reactions this assumption is not realistic because due to the equal projectile and target participation in the shocked zone, the local neutron excess is less than the average one. This problem indicates that the charge assymetry is an important ingredient of the evaporation model and so models which neglect this [17,30,31] cannot be applied to asymmetric collisions.

A similar consequence can be drawn from the large n/p ratio which goes up to 3 for large impact parameters (Table I). The collisions with large impact parameter dominate the inclusive cross sections where similarly high n/p ratios were obtained experimentally.[49]

V. Differential cross sections and correlations

Calculations were performed for $^{20}Ne + ^{238}U$ collisions at a projectile energy of 393 MeV/nucleon. In the triple differential cross sections strong azimuthal correlations are obtained at $\Delta\Phi=180^0$. The two main jets arise from the target and projectile evaporations, and can be observed as local peaks (Fig. 7) in the cross section at fixed impact parameter. The two peaks are approximately $\Delta\Theta=180^0$ from each other in the nucleus-nucleus CM frame because of momentum conservation. From the position of the peaks in the CM momentum space the momentum lost in the inelastic collision can be determined. Because of the lower temperatures of the projectile and target remnants at the break-up

moment, (Fig. 1) mainly heavier bound fragments, e.g. ^{4}He (Fig. 2), are formed here. Furthermore, because these are in thermal equilibrium with other species, their thermal velocities are considerably smaller than those of the lighter species and so the smearing due to the random thermal velocities is weaker while the collective velocities are the same. Thus the heavier fragment cross sections show the collective flow properties more clearly (Fig. 7), so that the deflection angle and the loss of collective momentum in the c.m. system are accurately measurable using the triple differential ^{4}He cross sections (Fig. 8).

Experimental triple differential (azimuth dependent) cross sections are not available yet, but p, d, and t double differential cross sections for central ($M_{tot} > 10$) Ne (393 MeV/N) + U reactions were measured recently.[2,3] Averaging over the azimuth angle in the triple differential cross sections given in Fig. 7 and integrating over b with the smooth cut-off (Fig. 3) we obtain the double differential cross sections in our model. The comparison to the experimental data shows an overall agreement with discrepancies remainingin some regions (Fig. 9). At small angles ($\Theta = 20^0 - 30^0$) the energy dependence in our calculation is stronger and also the sideward peaking is predicted at higher angles. Both of these deviations indicate that in the experiment the collisions with higher impact parameters have a larger weight than assumed by the smooth cut-off curve, or that the one fluid model overestimates somewhat the bounce-off angles at a given impact parameter. However, the forward suppression and sidewards peaking in the experimental and calculated data indicates the presence of the collective bounce-off process. Earlier speculations, that the forward supression in p spectra is caused by the formation of composite fragments does not hold, because the composite fragment cross sections (d,t) are also supressed in forward directions both in the experiment and in our calculation.

Recently azimuthal correlations between slow heavy and fast light fragments have also been measured.[4] The results show strong 180° azimuthal correlations providing a further experimental evidence for collective processes. In our model the correlation function [4] $R(\Phi)$ is defined on the basis of the triple differential cross section as:

$$R(\delta) = \frac{2\pi \int \sigma_{^4He}(90^0,\phi,\varepsilon)\, \sigma_p(40^0,\phi+\delta,30\text{-}40\ \text{MeV})\, d\phi\, d\varepsilon}{\int \sigma_{^4He}(90^0,\phi,\varepsilon)\, d\phi\, d\varepsilon \int \sigma_p(40^0,\phi+\delta,30\text{-}40\ \text{MeV})\, d\phi} - 1. \tag{20}$$

The experimentally observed 180° - azimuthal correlations are in qualitative agreement with the results of the calculations (Fig. 10). In our calculation this effect is caused by the collective bounce-off: The heavier fragments (^{4}He) are produced mainly on the colder target side and the protons on the opposite side. This $\Phi = 180°$ correlation between protons and heavy nuclei holds also for heavier fragments (target residues described in Sect. VI).

Neutron double differential cross sections are also available now for Ne (337 MeV/N) + U reactions and these can be compared to the proton cross sections measured at somewhat higher beam energies.[49] In Fig. 11 these experimental data are compared to our central Ne (393 MeV/N) + U calculations. The n/p ratio in our calculation increases less rapidly than the experimental ratios. This is mainly caused by the fact that the experiment is inclusive and peripferal collisions dominate at low energies. For such collisions we also have large n/p ratios (n/p ≃ 4 see Table I) but these are not taken into account in the cross sections for central collisions because of the smooth cut-off.

VI. Formation of heavy fragments in the framework of hydrodynamics

In the previous sections only the light fragment formation was discussed under the assumption that there is local thermal and chemical equilibrium between these fragments. However, this assumption is satisfactory only for the regions where we have a higher excitation energy at the break-up phase. There are other regions (mainly the "target residue") where the nucleons are bound deeper than -8 MeV and so light fragment formation is not possible. The fluid belonging to this deeply bound region are not taken into account in the calculation of the light fragment cross sections. This region is of considerable size compared to the whole reaction zone so that we have to choose an other description than in the previous section, since local equilibrium assumptions may not be applied.

In the most typical intermediate impact parameter region 10 - 30 % of the fluid cells forms a connected spatial region where the nucleons are deeply bound at break-up. We assume that the nucleons in this region form an intermediate nucleus with given mass and excitation energy. The mass of the nucleus is

$$A_{Bou.} = \int_{V_{Bou.}} d^3r \; n(r) \; , \tag{21}$$

where the integral runs over the fluid volume $V_{Bou.}$ where the internal excitation energy $\varepsilon < -8$ MeV/nucl. At the calculation of the total excitation energy of the heavy fragment we take into account the internal energy ε and the energy arising from the spread of the flow momenta in this region. We integrate the four momenta of the fluid cells $p(r) = (p(r), w(r))$

$$\begin{aligned} P &= \int d^3r \; p(r)\, n(r) = \int d^3r \; n(r)\, (m_n + \varepsilon(r))\, \gamma(r)\, v(r), \\ W &= \int d^3r \; w(r)\, n(r) = \int d^3r \; n(r)\, (m_n + \varepsilon(r))\, \gamma(r), \end{aligned} \tag{22}$$

where $\gamma(r) = 1/\sqrt{(1-v(r)^2)}$. In this way we can get the rest mass of the heavy fragment as:

$$M_o = \sqrt{(W^2 - P^2)} \; , \tag{23}$$

and its specific excitation energy above the ground state (-8 MeV) :

$$E^* = (M_o - m_n A_{Bou.}) / A_{Bou.} + 8 \text{ MeV/N}. \tag{24}$$

This heavy fragment is expected to be emitted with a recoil energy E_R corresponding to the velocity:

$$\beta = P / W \; . \tag{25}$$

Thus we can get a rough estimate of the properties of the created heavy residue. The underlying basic idea is very similar to the abrasion-ablation model.[40] However, we are not bound to the straight line geometry, the recoil has a transverse component and we can determine the excitation energy of the residue without any additional assumption. We neglected, however, certain processes e.g. the excitation stemming from the deformation of the spatial region where the deeply bound nucleons are situated at the break-up moment and the excitation arising from the sharp cut-off of the density at the surface.

Thus we underestimate the excitation energy by a few MeV/N. On the other hand due to the rough grid the accuracy of the predicted mass is of the order of the mass contained in the fluid cells at the surface of the deeply bound region, which form a layer of width ≃ Δx/2. This yields an essential relative error especially for smaller residues:

$$\Delta A / A \simeq (9\pi\, n / 2A)^{1/3}\ \Delta x/2 \simeq 0.67\, A^{-1/3} \qquad (26)$$

Such excited target residues have been found recently in ^{12}C (84 MeV/N) + induced reactions [51-52] around A ≃ 50 (ΔA≃10) with a recoil energy of about 1 MeV/N (β≃0.04-0.05c). The small spread of the mass spectrum indicates that these are not fission products, and evaporation calculations show that these final states may arise from an excited intermediate compound nucleus of A≃90 and E^{*}≃8 MeV/N. Such excited compound nuclei are also predicted by the hydrodynamic model.

The recoil energy versus the mass of the residue is plotted in Fig. 12. The low energy (E_R) residues are expected from peripferal collisions (b>5 fm) in the hydrodynamic model, while residues with large recoil energy are formed in central collisions. We get higher masses for these residues than the experimentally observed masses, but we calculate the excited intermediate states only. The final deexcitation of these nuclei might easily result in a further mass loss of ΔA ≃ 10 which would make it close to the experiment. We underestimate the collective recoil energy of these fragments by 15 -20 % . This latter difference might be caused by final state interactions (absorption of light fragments emitted from the hot compressed region after the break-up) which are not included in our simplified model. However, the accuracy of our calculations is also not much better than 15 - 20 % , as we mentioned already, so refinements in these details would not be reasonable.

In Fig. 13 the recoil angle Θ is plotted versus the mass of the target residue. The recoil angle increases with impact parameter in both reactions we studied. At 393 MeV/N projectile energy the residues belonging to the lowest impact parameters have high excitation energy so that they probably cannot be observed as one heavy residue (Table II). At high impact parameters the fluctuations and final state interaction effects are large compared to our recoil energy so that our estimated recoil angles and energies are not observable. Nevertheless, in an intermediate impact parameter region there should be a cor-

relation between the residue mass and the mean recoil angle. For the ^{12}C + ^{124}Sn reaction we expect an enhancement at $\Theta \approx 50 - 60^0$ for the residue masses around A = 60 - 70, caused basically by the collective bounce-off process,[14] which acts strongly at intermediate impact parameters. Experiments for ^{12}C + ^{124}Sn reaction[51] show a shoulder at $\Theta = 60^0$ in the angular distribution of the residues with large mass deficiency. According to our calculations this might be a consequence of the collective bounce-off process.

In Table II the mass, excitation energy and emission angle of the expected heavy residue are shown versus the impact parameter. In a wide impact parameter range we get an intermediate nucleus with relatively small (a few Mev/nucl.) excitation energy. These intermediate states may decay by light fragment or nucleon emission to yield a somewhat lighter observable heavy fragment. These final fragment states will be in the vicinity of the intermediate state on the (N,Z) plane. In Fig. 14 the intermediate residues are shown on the (N,Z) plane for several impact parameters in a Ne + U reaction at 393 MeV/nucleon bombarding energy. These results indicate that in reactions with heavy target or projectile new heavier neutron rich isotopes might be produced similarly to the already observed lighter ones arising from projectile fragmentation.[53]

The model of the residue formation presented here does not work at small and at very large impact parameters. At small impact parameters the intermediate residue has a large excitation energy. This is caused by the fact that the deeply bound cells do not occupy a singly connected spatial region, but rather a ring or two or more separate connected regions. The flow velocity differences between different parts of the deeply bound region become large and this is the reason of the apparent higher excitation energies. In this case the intermediate residue fissions into two or more parts or it may be that already at the break-up moment the deeply bound cells form several fragments. The latter happens at large impact parameters also, where both target and projectile residues are present. However, for these large impact parameters the participant zone is already very small and contains only a few nucleons, so that the hydrodynamic description looses its validity and other processes as microscopic n-n correlations become more important.[5,46]

VII. Event by event analysis

Recently, for the investigation of the possible collective properties several methods are introduced like sphericity tensor, energy flow tensor, thrust analsis.[54-58] The first experimental studies with the Plastic Ball[48] and with streamer chamber[59] are in progress.

Theoretically it is straightforward to evaluate the real symmetric sphericity matrix in the CM frame :

$$M_{\alpha\beta} = \Sigma_i \, p_{i\alpha} \, p_{i\beta} \, , \qquad \alpha,\beta = x,y,z \tag{27}$$

where i runs over all emitted charged particles (up to ^{4}He for the Plastic Ball experiments and in our calculations). The eigenvalues Q_i and eigenvectors e_1, e_2, e_3 of the tensor can be determined. If we normalize the sum of eigenvalues to unity so that $Q_3 > Q_2 > Q_1$ we can evaluate the commonly used quantities: sphericity [54] $S = 1.5(Q_1 + Q_2)$, flatness $F = \sqrt{3}\,(Q_2 - Q_1)/2$, jet angle Θ_{CM} = arc cos($[\, e_3]_z$ / e_3), and aspect ratios [58] $R_1 = Q_3/Q_1$ and $R_2 = Q_2/Q_1$.

Before the discussion of the calculational details let us emphasize two problems. Most detectors does not detect neutrons, and these need not have the same distribution as the average of the other light charged fragments. Similarly heavy clusters and residues are also not detected. Therefore, to gain a result which is comparable to experiments the analysis of the cluster formation is unavoidable.

From the final momentum distribution of the light fragments ${}^1_jF_H$ (see Sect. III. Eq.(12,13)) the spericity tensor can be obtained as

$$M_{\alpha\beta} = \int d^3r \; \Sigma_{j_{clust.}} \int d^3P^{CM} \, [\, {}^1_jF^{CM}_H(P^{CM}, r) \,] \, P^{CM}_{j\alpha} \, P^{CM}_{j\beta} \tag{28}$$

This expression (28) can be simplified [60] and separated into a thermal and a flow term. The importance of the thermal therm arising from this separation is discussed in Ref. 60.

In Fig. 15 the jet angle and the sphericity are shown for different impact parameters for protons, alpha particles, and for the sum of all light

charged fragments up to ^{4}He. We have seen in the angular distributions that the ^{4}He particles show the collective jet structure stronger than the protons. Their sphericity parameters, however, are not essentially different from those of the protons because the structure of the ^{4}He cross section may be observed best at higher energies (E= 200-300 MeV/N) where the cross section is two or three orders of magnitude smaller than at low energies. So the calculated sphericity values for ^{4}He are determined mainly by low energy particles. The low energy cut-off of the Plastic Ball has the advantage of excluding the almost isotropic low energy target evaporation and so the structure of the cross section might show up more strongly in the global variables. The calculated jet angles are somewhat larger than in the cascade calculations of Ref. 58.

In Fig. 15 the sphericity and flatness parameters (S,F) of the emitted light fragments calculated with and without the thermal momenta (I, I-t) are compared to each other. The thermal smearing increases the sphericity by 0.15-0.2 and decreases the flatness by 20-30% at small and intermediate impact parameters. This indicates that in earlier theoretical global flow analyses of Ref. 56 the neglection of thermal smearing effects lead to an overestimation of the thrust value.

In a comparision of our calculations with the experiments some difficulties arise. The limited sensitivity of the detector in momentum space and the fact that most detectors do not cover a spherically symmetric region around the CM in the momentum space causes serious problems. The sphericity matrix detected by a given detector is not equal to the one defined by Eq.(28) but rather is given by:

$$M_{\alpha\beta} = \int d^3r \sum_{j_{clust.}} \int_{\mu_{pb}} d^3P^{CM} \left[{}_jF^{CM}(P^{CM},r) \right] P^{CM}_{j\alpha} P^{CM}_{j\beta} , \tag{29}$$

where μ_{pb} is the sensitivity region of the detector in the momentum space. Unfortunately, owing to the separation introduced [60] we are not able to reproduce easily such a restriction.

Fig. 16 might provide, however, an insight into this problem. The rapidity distribution of the alpha particles is shown in the reaction plane for a Ne (393 MeV/N) + U calculation together with the acceptance of the Plastic Ball. [48] The local maximum of the cross section caused by the evaporation of the bounced off projectile lies at the upper energy limit of the Plastic Ball for full particle identification (≈ 250-300 MeV/N) due to the fact that the

collision is higly inelastic. The peaked structure of the cross section would show up in the Plastic Ball observables the better the closer the projectile energy is to this upper energy limit (i.e. at 300-400 MeV/N). At very high projectile energies, in the GeV/n region, the fluctuations and the effects arising from the special sensitivity range of the detector are probably too strong to allow for a determination of the collective flow variables.

Because of these difficulties a Monte Carlo simulation would be extremely useful where for some previously given emission patterns the sphericity and jet angle variables were evaluated in exactly the same way and with all restrictions as it is done with the actual experimental device.

VIII. Conclusions

We have presented results of an extended fluid-dynamical model which incorporated the formation of light nuclear fragments and their final thermal evaporation. As we have seen in the previous sections there are numerous signatures of the collective flow processes observable in the fragment emission as i) the sidewards peaked structure of the double differential cross sections especially for composite fragments, ii) the correlations arising from the collective structure of the triple differential cross sections both between two protons,[5,46] and light and heavy fragments, iii) the high energy component in the recoiled target residues, and iv) the large jet angles in the global analysis of the central events. These experimental signatures provide evidence for the existence of a collective flow of the hot, dense nuclear matter formed in relativistic heavy ion collisions.[61] These collective processes are governed by the underlying equation of state and transport properties of the nuclear, hadronic or quark matter. The detailed study of the composite fragment cross sections in 4π exclusive experiments to be completed in the near future may provide a unique tool for the determination of the properties of strongly interacting matter at extreme conditions and may allow for a determination of phase transitions in dense nuclear matter.[62] We are looking forward to the analysis of 4π experiments presently underway.

Enlightening discussions with H. H. Gutbrod and H. G. Ritter are gratefully acknowledged. The authors thank J. Blachot and V.D. Toneev for the communication of their results prior to publication. This work is supported by the Alexander von Humboldt Stiftung, by the Bundesministerium für Forschung und Technologie and by the Gesellschaft für Schwerionenforschung.

References

1.) H.G. Baumgardt, J.U. Schott, Y. Sakamoto, E. Schopper, H. Stöcker, J. Hofmann, W. Scheid, W. Greiner, Z. Phys. A273 (1975) 359 and J. Hofmann, H. Stöcker, U. Heinz, W.Scheid, W. Greiner; Phys. Rev. Lett. 36 (1976) 88; H.G. Baumgardt, E. Schopper, J. Phys. Lett. G5 (1979) L231.

2.) R. Stock, H.H. Gutbrod, W.G. Meyer, A.M. Poskanzer, A. Sandoval, J. Gosset, C.H. King, G. King, Ch. Lukner, Nguyen Van Sen, G.D. Westfall, K.L. Wolf, Phys. Rev. Lett. 44 (1980) 1243.

3.) H.H. Gutbrod, Lawrence Berkeley Laboratory Rep. LBL-11123(1980) Proc. of Symp. on High Energy Nuclear Int. Hakone, Japan ed.: K.Nakai and A.S. Goldhaber, July 7-11, (1980) p. 93.

4.) W.G. Meyer, H.H. Gutbrod, Ch. Lukner, A. Sandoval, Phys. Rev. C22 (1980) 179.

5.) L.P. Csernai, W. Greiner, H. Stöcker, I. Tanihata, S. Nagamiya, J. Knoll, Phys. Rev. C (1982) in press (code: CM 2005); I. Tanihata, Proc. of Symp. on High Energy Nuclear Int. Hakone, Japan ed.: K.Nakai and A.S. Goldhaber, July 7-11, (1980) p. 382.

6.) L.P. Csernai, H.W. Barz, Z. Phys. A296 (1980) 173.

7.) J. Hofmann, W.Scheid, W. Greiner, Nuovo Cimento 33A (1976) 343; J.A. Maruhn, T.A. Welton, C.Y. Wong, J. Comp. Phys. 20 (1976) 326; J. Hofmann, H. Stöcker, U. Heinz, W. Scheid, W. Greiner, Phys. Rev. Lett. 36 (1976) 88; J.A. Maruhn, Proc. Top. Conf. on Heavy Ion Collisions, Fall Creek Falls State Park, Tennessee (1976) p.156

8.) A.A. Amsden, G.F.Bertsch, F.H. Harlow, J.R. Nix, Phys. Rev. Lett. 35 (1975) 905; A.A. Amsden, F.H. Harlow, J.R. Nix, Phys.Rev. C15 (1977) 2059; A.A. Amsden et al., Phys.Rev. Lett. 38 (1977) 1155; J.R. Nix, D. Strottman, Phys. Rev. C23 (1981) 2548.

9.) H. Stöcker, W. Greiner, W. Scheid, Z. Phys. A286 (1978) 121; H. Stöcker, J.A. Maruhn, W. Greiner, Z. Phys. A290 (1979) 297; H. Stöcker, R.Y.Cusson, J.A.Maruhn, W. Greiner, Z. Phys. A294(1980)125; H. Stöcker, J.Hofmann, J.A. Maruhn, W. Greiner, Prog. Part. Nucl. Phys. 4 (1980) 125.

10.) P. Danielewicz, Nucl. Phys. A314 (1979) 465.

11.) L.P. Csernai, B.Lukács,J.Zimányi, Nuovo Cim.Lett. 27(1980) 111.

12.) H.H. Tang, C.Y. Wong, Phys.Rev. C21 (1980) 1846.

13.) G. Buchwald, L.P. Csernai, J.Maruhn, W. Greiner, H. Stöcker, Phys. Rev. C24 (1981) 135; G. Buchwald, L.P. Csernai, G.Graebner, J.Maruhn, W.Greiner, H. Stöcker, Z. Phys. A303 (1981) 111; G. Buchwald et al., to be published

14.) H. Stöcker, J.Maruhn, W. Greiner, Phys.Rev. Lett. 44 (1980) 725 and Z. Phys. A293 (1979) 173.

15.) H. Stöcker, L.P. Csernai, G. Graebner, G. Buchwald, H. Kruse, R.Y. Cusson, J.A. Maruhn, W. Greiner, Phys. Rev. C (1982) in press (code: LC2009C); H. Stöcker et al. Phys. Rev. Lett. 47 (1981) 1807.

16.) A.J. Sierk, J.R. Nix, Phys. Rev. C22 (1980) 1920.

17.) J.I. Kapusta D. Strottman, Phys. Rev. C23 (1981) 1282.

18.) G.F. Bertsch and A.A. Amsden, Phys. Rev. C18 (1978) 1293.

19.) G.Westfall, J.Gosset, P.J.Johansen, A.M. Poskanzer, W.G. Meyer, H.H. Gutbrod, A. Sandoval, R. Stock, Phys. Rev. Lett. 37 (1976) 1202; J. Gosset, H.H. Gutbrod, W.G. Meyer, A.M. Poskanzer, A. Sandoval, R. Stock, G. Westfall, Phys. Rev. C16 (1977) 629.

20.) J.Gosset, J.I. Kapusta and D. Westfall, Phys. Rev. C18 (1978) 844.

21.) I. Tanihata, S. Nagamiya, S. Schnetzer, H. Steiner, Phys. Lett. 100B (1981) 121.

22.) J.D. Stevenson, J. Martins, P.B. Price, Phys. Rev. Lett. 47 (1981) 990.

23.) S. Nagamiya, M.-C. Lemaire, E. Moeller, S. Schnetzer, G. Shapiro, H. Steiner, I. Tanihata, Phys. Rev. C24 (1981) 971.

24.) Gy. Fái, J. Randrup, Lawrence Berkeley Laboratory rep. LBL-13357 (81) (1981); J. Randrup and S.E. Koonin, Nucl. Phys. A356 (1981) 223.

25.) P.J. Siemens and J.I. Kapusta, Phys. Rev. Lett. 43 (1979) 1486.

26.) A. Z. Mekjian, Phys. Rev. Lett. 38 (1977) 640; Phys. Rev. C17 (1978) 1051; Nucl. Phys. A312 (1978) 491.

27.) P.R. Subramanian, L.P. Csernai, H. Stöcker, J.A. Maruhn, W. Greiner and H. Kruse, J. Phys. G7 (1981) 1241.

28.) S. Das Gupta and A. Z. Mekjian, Phys. Rep. 72 (1981) 131.

29.) J.I. Kapusta, Phys. Rev. C16 (1977) 1493.

30.) G. Röpke, L. Münchow, H. Schulz, Phys. Lett. 110B (1982) 21.

31.) J. Knoll, L. Münchow, G. Röpke, H. Schulz, Phys Lett. in press

32.) T. Bíró, H. W. Barz, B. Lukács and J. Zimányi, Central Research Institute for Physics Budapest Report No. KFKI-1981-90.

33.) H. Stöcker, Lawrence Berkeley Laboratory Report No. LBL-12302 (1981)

34.) H. Stocker, A.A. Ogloblin, W. Greiner, Z. Phys. A303 (1981) 259.

35.) P.J. Siemens and J.O. Rasmussen, Phys.Rev. Lett. 42 (1979) 880.

36.) I. Montvay and J. Zimányi, Nucl. Phys. A316 (1979) 490; H.W. Barz, B. Lukács, J. Zimányi, Gy. Fái and B. Jakobsson, Z. Phys. A302 (1981) 73.

37.) A.A. Amsden, A.S.Goldhaber, F.H. Harlow, J.R. Nix, Phys. Rev. C17 (1978) 2080.

38.) L.P. Csernai, I. Lovas, J.A. Maruhn, A. Rosenhauer, J. Zimányi, and W. Greiner, UFTP 64/1981 Subm. to Phys. Rev. C (code. CM2035)

39.) L.P. Csernai and H. Stöcker, Phys. Rev. C (1982) in press (code: CXK137)

40.) W. Scheid, H. Müller, W. Greiner, Phys. Rev. Lett. 32 (1974) 741.

41.) J.I. Kapusta, Phys. Rev. C24 (1981) 2545; ibid. C21 (1980) 1301.

42.) H.W. Barz, L.P. Csernai, W. Greiner, Phys. Rev. C (1982) in press (code: CFI 210)

43.) L.P. Csernai, D. Kisdi and J. Németh, Acta Phys. Hung. 38 (1975) 89.

44.) D. K. Scott, Proc. Int. Workshop on Gross Properties of Nuclei and Nuclear Excitations X. Hirschegg, Jan. 18-23, 1982, ed. by H. Feldmeier (TH Darmstadt 1982) in press; R.K. Tripathi, Phys. Rev. C25 (1982) 1114.

45.) P. Marmier, E. Scheldon: Physics of Nuclei and Particles (New York, Academic Press) Vol II pp. 886, 920, 935.

46.) L.P. Csernai, W. Greiner, Phys. Lett. 99B (1981) 85.

47.) V. D. Toneev, private communication

48.) H.H. Gutbrod, H.G. Ritter GSI Nachrichten 1-1982 (1982) p. 3;and private communication

49.) R.A. Cecil, B.D. Anderson, A.R. Baldwin, R. Madey; Phys. Rev. C24 (1981) 2013; W. Schimmeling, J.W. Kast, D. Orthendal, R. Madey, R.A. Cecil, B.D. Anderson and A.R. Baldwin, Phys. Rev. Lett. 43 (1979) 1985.

50.) J.D. Bowman, W.J. Swiatecki and C.F. Tsang, unpublished

51.) J. Blachot, J. Cracon, A.Lleres, A.Gizon, H. Nifenecker, Proc. Int. Workshop on Gross Properties of Nuclei and Nuclear Excitations X. Hirschegg, Jan. 18-23, 1982, ed. by H. Feldmeier (TH Darmstadt 1982) in press; J. Blachot, J. Crancon, J.Genevey, A. Gizon, A. Lleres; Z. Phys. A 301 (1981) 91; J. Blachot, J. Crancon, H. Nifenecker, A. Lleres, A. Gizon, J. Genevey, Z. Phys A 303 (1981) 85; and J. Blachot private communication.

52.) A. Fleury, H. Delagrange, R. del Moral, J.P. Dufour, F. Hubert, M.B. Mauhourat, Y. Llabador, Contribution to the Xth European Conf. on the Physics and Chemistry of complex Nuclear Reactions. Lillehammer, Norway, August 1981 (unpublished)

53.) T.J.M. Symons, V.P. Viyogi, G.D. Westfall, P. Doll, D. E. Greiner, H. Faraggi, P.J. Lindstrom, D.K. Scott, H.J. Crawford, C. McParland, Phys. Rev. Lett. 42 (1979) 40; G.D. Westfall, T.J.M. Symons, D. E. Greiner, H.H. Heckmann, P.J. Lindstrom, J. Mahoney, A.C. Schotter, D.K. Scott, H.J. Crawford, C. McParland, T.C. Aves, C.K. Gelbke, J.M. Kidd, Phys. Rev. Lett. 43 (1979) 1859.

54.) J.D. Bjorken, S. J. Brodsky, Phys. Rev. D1 (1970) 1416.

55.) E.Farhi, Phys. Rev. Lett. 39 (1977) 1587.

56.) J. Kapusta, D. Strottman, Phys. Lett. B106 (1981) 33.

57.) J. Cugnon, J. Knoll, C. Riedel, Y Yariv, Phys.Lett. B109 (1982) 167.

58.) M. Gyulassy, K.A. Frankel, H. Stöcker, Lawrence Berkeley Laboratory Rep. No. LBL - 13379 (1981) Subm. to Phys. Lett.

59.) H. Ströbele et al., to be published; and J.W. Harris, R. Brockmann, R.E. Renfordt, F. Riess, A. Sandoval, H. Stöbele, R. Stock, J. Miller, H.G. Pugh, M. Raff, L.S. Schroeder and K.L. Wolf, Bull. of APS 26 (1981) 1112.

60.) H. Stöcker et al., to be published

61.) W. Greiner; Proc. of the 3rd Adriatic Europhysics Study Conf. on the Dynamics of the Heavy Ion Collisions, Hvar, Yugoslavia, May 25-30, 1981 (North-Holland 1981) p. 359.

62.) M. Gyulassy, W. Greiner, Ann. Phys. 109 (1977) 485.

Table I: (a) Total light fragment multiplicities for the Ne + U (393 MeV/N) reaction calculated in the hydrodynamic and evaporation model (with B_o=-16 MeV, K_o= 400 MeV, η= 10 MeV/fm^{2}c) at different impact parameters b. The average density (ρ), internal energy (ε), temperature(T) and the specific entropy before (σ) and after (σ') the break-up process are also listed. The quantities T and σ' do not contain the contribution of the deeply bound fluid cells which form a heavy residue in the model (see Sect. VI).

b	ρ	ε	σ'	σ	T	p	n	d	t	^{3}He	^{4}He
fm	fm^{-3}	MeV/N			MeV						
0	0.053	0.71	1.76	1.90	11.6	10.5	34.4	7.7	24.5	3.0	18.4
1	0.054	0.38	1.72	1.79	11.4	9.1	30.2	6.7	22.2	2.6	16.7
2	0.063	0.09	1.70	1.76	11.3	8.6	30.6	5.7	22.1	2.2	19.1
3	0.071	0.08	1.63	1.70	11.2	8.3	28.0	5.1	20.5	2.0	17.1
4	0.079	-1.05	1.49	1.66	11.4	7.7	25.0	4.4	18.4	1.7	15.2
5	0.087	-1.49	1.40	1.64	12.5	7.6	23.4	3.7	16.7	1.4	13.9
6	0.098	-2.32	1.17	1.60	13.7	8.1	24.1	3.1	14.9	1.3	13.7
7	0.101	-4.20	1.01	1.65	15.1	7.1	19.5	2.7	11.8	1.1	9.6
8	0.108	-6.40	0.84	1.67	13.4	4.3	13.1	1.8	7.3	0.7	7.1

(b) Total light fragment multiplicities for Ne + Pb (800 MeV/N) reaction.

b	ρ	ε	σ'	σ	T	p	n	d	t	^{3}He	^{4}He
fm	fm^{-3}	MeV/N			MeV						
0	0.055	15.1	2.45	2.66	23.6	24.4	45.8	9.0	21.3	3.9	9.3
1	0.058	14.2	2.40	2.61	23.7	25.6	47.7	9.0	23.6	4.0	10.4
2	0.055	12.5	2.40	2.57	21.3	21.6	41.9	8.7	21.0	3.7	10.1
3	0.056	11.0	2.31	2.38	20.0	19.5	38.7	7.8	21.7	3.3	11.5
4	0.059	8.6	2.16	2.22	18.0	16.7	35.0	6.9	21.8	2.9	13.3
5	0.066	6.4	1.91	2.07	16.3	14.1	31.6	5.6	20.5	2.4	14.8
6	0.068	3.2	1.62	1.80	13.8	12.1	30.7	5.0	20.2	2.0	17.8
7	0.075	0.6	1.28	1.62	11.5	8.8	26.0	4.0	18.0	1.4	18.4
8	0.083	-2.1	0.97	1.41	9.7	6.0	20.7	2.9	12.9	1.0	15.8

Table II: (a) Parameters of the intermediate excited target residues for the Ne + U (393 MeV/N) reaction calculated in the hydrodynamic and evaporation model (B_o=-16 MeV, K_o= 400 MeV, η= 10 MeV/fm²c) at different impact parameters b. The expected mass $A_{Bou.}$, recoil angle θ, recoil energy E_R, excitation energy E^* (without surface and deformation energies) and recoil velocity β. The values in brackets are unphysical because of the large excitation energy or the large fluctuations of the recoil direction.

b	$A_{Bou.}$	θ	E_R	E^*	β
fm		degr.	MeV	MeV/N	c
0	(49)	(1)	(161)	(7.4)	(0.083)
1	(56)	(3)	(200)	(11.1)	(0.087)
2	51	26	169	3.5	0.084
3	73	57	134	2.7	0.063
4	97	63	95	0.1	0.046
5	116	86	37	-1.2	0.026
6	140	(90)	(13)	-2.8	(0.014)
7	179	(90)	(9)	-3.1	(0.010)
8	204	(90)	(8)	-3.1	(0.009)

(b) Parameters of the intermediate excited target target residues for ^{12}C + ^{124}Sn (86 MeV/N) reaction (with B_o=-16 MeV, K_o= 400 MeV, η= 20 MeV/fm²c) at different impact parameters.

b	$A_{Bou.}$	θ	E_R	E^*	β
fm		degr.	MeV	MeV/N	c
0	71	0	45	0.6	0.037
1	72	10	39	-0.5	0.034
2	72	21	33	-1.5	0.031
3	73	43	25	-2.3	0.027
4	80	50	18	-3.4	0.022
5	90	68	11	-3.3	0.016
6	96	75	3	-3.8	0.008
7	101	(90)	(2)	-4.5	(0.006)

Figure Captions

Figure 1: Density (ρ) temperature (T) and velocity (arrows) distributions in a relativistic heavy ion collision (Ne + U 393 MeV/N) in the lab system at the break-up moment (t= 26fm/c). The impact parameter of the collision is b=6fm. The crosses indicate that the flow velocity is $v < 0.1$ c. The full contour lines belong to temperatures T=10,20 MeV, the dashed ones to nucleon densities ρ= 0.05, 0.1 ($1/fm^3$).

Figure 2: Proton (p) and alpha particle (α) density contour lines calculated for the break-up configuration of Fig. 1. The protons are formed in the midle hot regions mainly opposite to alphas which are formed at the sides. The contour lines belong to n_α = 0.005 ($1/fm^3$), n_p = 0.003, 0.006 ($1/fm^3$).

Figure 3: The central (high multiplicity selected) cross sections are calculated by using the the cascade simulations of Toneev[47] (dashed line). Collisions with high impact parameters also contribute to the high multiplicity selected data. The plotted smooth cut-off function was used for the calculation of the contributions from different impact parameters in central reaction cross sections in the framework of the hydrodynamic and evaporation model.

Figure 4: Energy spectra of light fragments in a central Ne (393 MeV/N) + U reaction. The assumed lower energy cuts in the recent preliminary Plastic Ball multiplicity measurements are indicated. [48] The average acceptances are estimated for this reaction on the basis of these calculated results by taking the ratio of the observable particles (in the high energy tail above the cut) to all emitted particles, neglecting variations with the impact parameter.

Figure 5: Bound proton multiplicities versus free proton multiplicities calculated in the hydrodynamic model (points) for different impact parameters. The error bars indicate the estimated thermal fluctuations together with the fluctuations arising from the limited sensitivity as described in Sect. IV. The data reduced by the estimated acceptances are given by triangles for the Ne (393 MeV/N) + U reaction too. For qualitative comparision preliminary experimental data [48] are shown. The data for small impact parameters agree with the experimental ones, while at high impact parameters the bound proton multiplicity is overestimated.

Figure 6: Light particle multiplicities (values reduced by the estimated acceptances) versus the total light fragment multiplicity calculated in the hydrodynamic and evaporation model for different impact parameters b=0-9fm for the Ne+Pb reaction at 800 MeV/N beam energy. In brackets the estimated acceptances are indicated. Apart from the higher acceptance, the reason of the higher ^{3}H than ^{3}He multiplicities is in the assumed large neutron excess of the evaporating matter.

Figure 7: Contour plots of triple differential invariant cross sections $(1/p)d^3N/dEd\Phi d\cos\theta$ for the reaction ^{20}Ne(393 MeV/N) + ^{238}U at impact parameter b = 6 fm in the reaction plane (Φ= 0°/180°) and in the plane orthogonal to it (Φ=90°). The contour lines labelled by parameter q correspond to a value of $10^q/(sr\ MeV^2)$. Figures a, b, c, d, e, f are corresponding to p, n, d, t, ^{3}He, ^{4}He cross sections respectively. The bounce-off effect is predominantly observable in t, ^{3}He and ^{4}He spectra

Figure 8: The dependence of the c.m. bounce-off deflection angle and inelasticity on the impact parameter b. At impact parameters lower than 3 fm the second local maximum of the spectrum vanishes and so the inelasticity cannot be uniquely determined, but the bounce off angle is measurable.

Figure 9: Double differential p, d, t cross sections for central Ne (393 MeV/N) + U reaction. The experimental cross sections [2,3] (points) are at 12, 21, 47, 82 MeV/N energies and the calculated ones at 10, 20, 50, and 80 MeV/N.

Figure 10: Heavy-light fragment correlations calculated in the theoretical model for one impact parameter b = 6 fm. The heavy fragment is ^{4}He at θ=90° in the lab system measured in coincidence with a proton at θ=40° in the energy range 30-50 MeV. The correlation at $\Delta\Phi$ = 180° is the consequence of the bounce-off effect. The experimental points are taken from Ref. 4.

Figure 11: Neutron double differential cross sections calculated for the central Ne (393 MeV/N) + U reaction together with experimental data from Ref. 49.

Figure 12: The recoil energy E_R versus the mass $A_{Bou.}$. of the heavy target residue for two reactions. The lower mass target residues have high recoil energy, E_R= 25-45 MeV. These decrease with the increasing mass of the residue in qualitative agreement with the observations of Ref. 51 (points) for the ^{12}C + ^{124}Sn (86 MeV/N) reaction.

Figure 13: The recoil angle Θ_{lab} versus the mass $A_{Bou.}$ of the heavy residue. At large impact parameters the the recoil velocity is relatively small compared to fluctuations. So although the expectation of the deflection angle is around 90° the fluctuations and final state interactions probably yield a flat distribution.

Figure 14: The estimated position of the intermediate compound target residue on the [N,Z] plane from the hydrodynamic model. The N to Z ratio is that of Uranium. The neutron rich excited heavy residues can decay mainly by p, n and α emission and so the final states are in a narrow region ($\Delta A \approx 4$-6) around the indicated line. In this way neutron rich isotopes might be produced.

Figure 15: Calculated sphericity S and flatness F versus the jet angle Θ_{cm} for different impact parameters in the Ne(393 MeV/N) + U reaction plotted separately for protons p, (crosses) alpha particles α (open squares) and all charged light fragments (open circles and triangles). The lines indicated by full dots and triangles (l-t) represent the sphericity and flatness of the light particles without thermal smearing.

Figure 16: Contour plot of the calculated triple differential invariant ^{4}He cros section for the Ne (393 MeV/N) + U reaction at impact parameter b=6fm. Two peaks arise from the target and projectile evaporations. The dashed lines indicate the Plastic Ball and Plastic Wall response taken from Ref. 48. The full determination of particles is possible in the region indicated by (Z,A,E) so that the experimental determination of the matrix M is restricted to this region. The energy flow matrix [59] can be determined, however, by using the information from the interior layer, labelled by E, too. The maximum arising from the projectile evaporation is detectable in the above reaction by the Plastic Ball.[48]

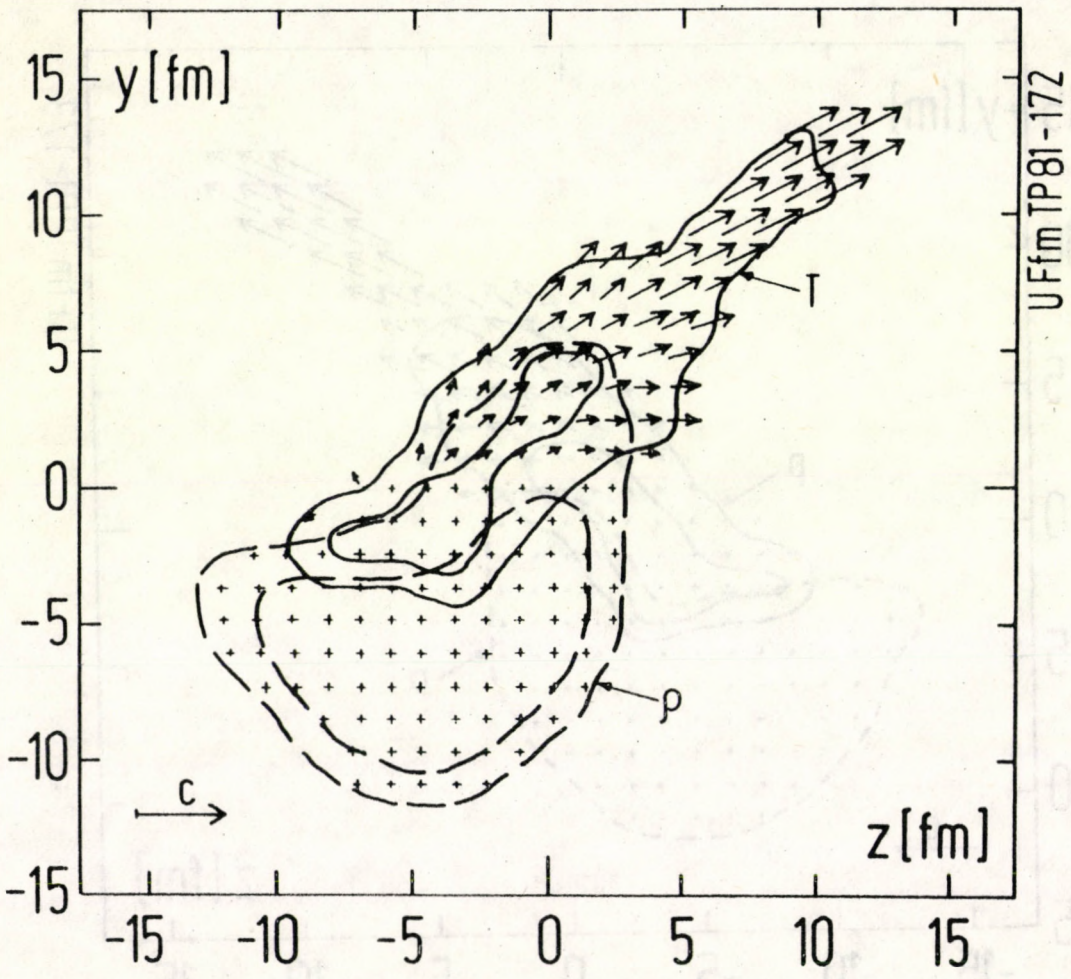

Fig. 1

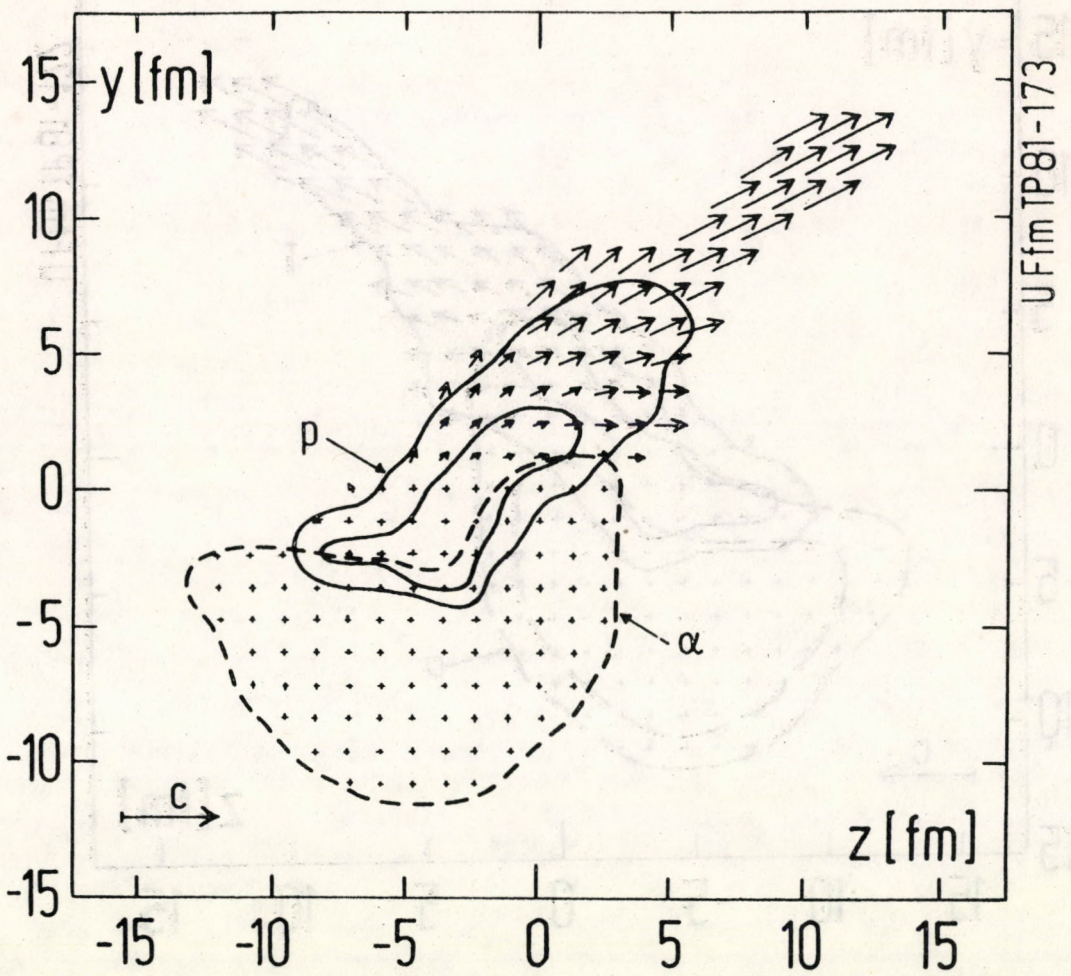

Fig. 2

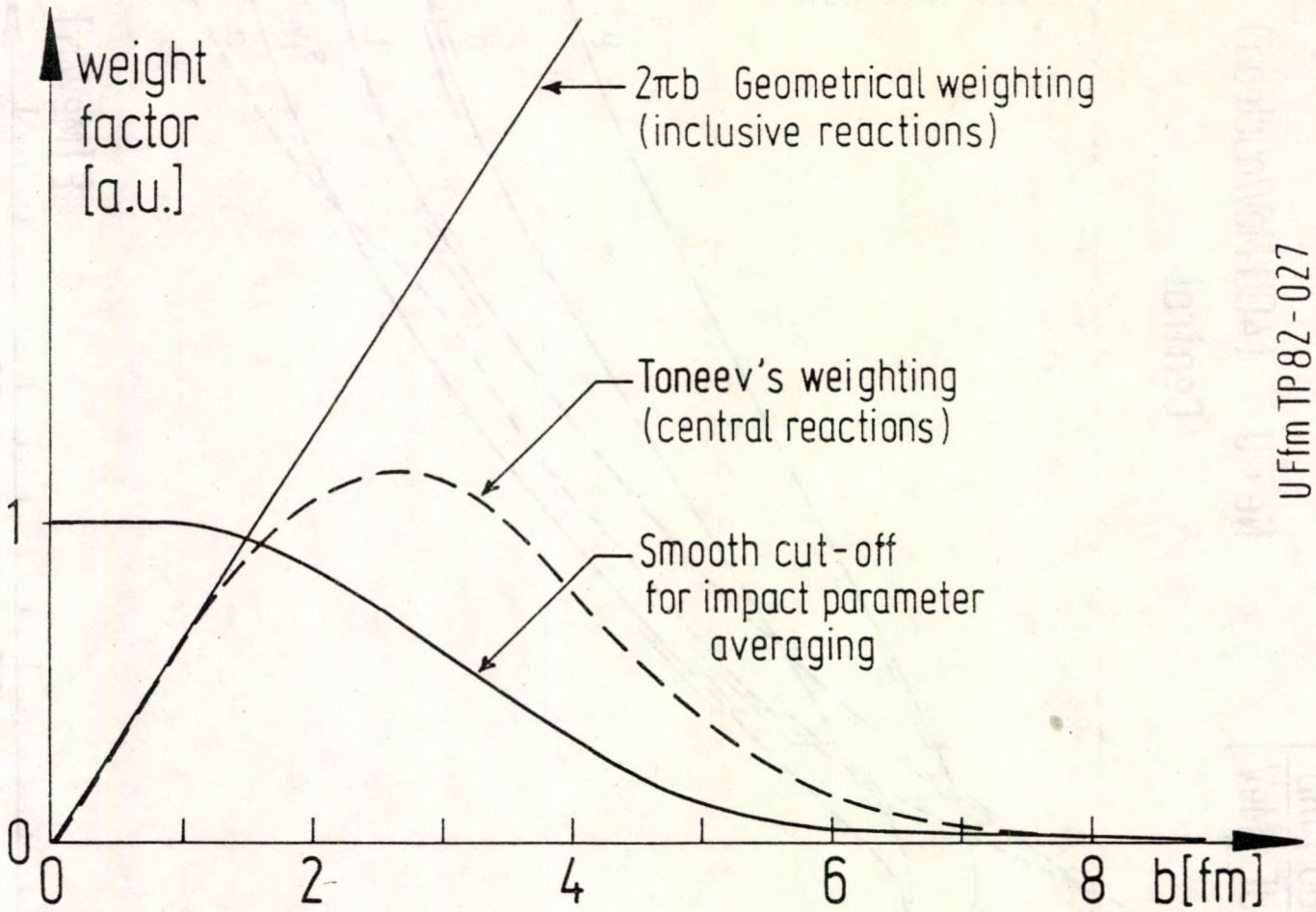
weight
factor
[a.u.]
2πb Geometrical weighting
(inclusive reactions)
Toneev's weighting
(central reactions)
Smooth cut-off
for impact parameter
averaging
1
0
0
2
4
6
8
b[fm]

Fig. 3

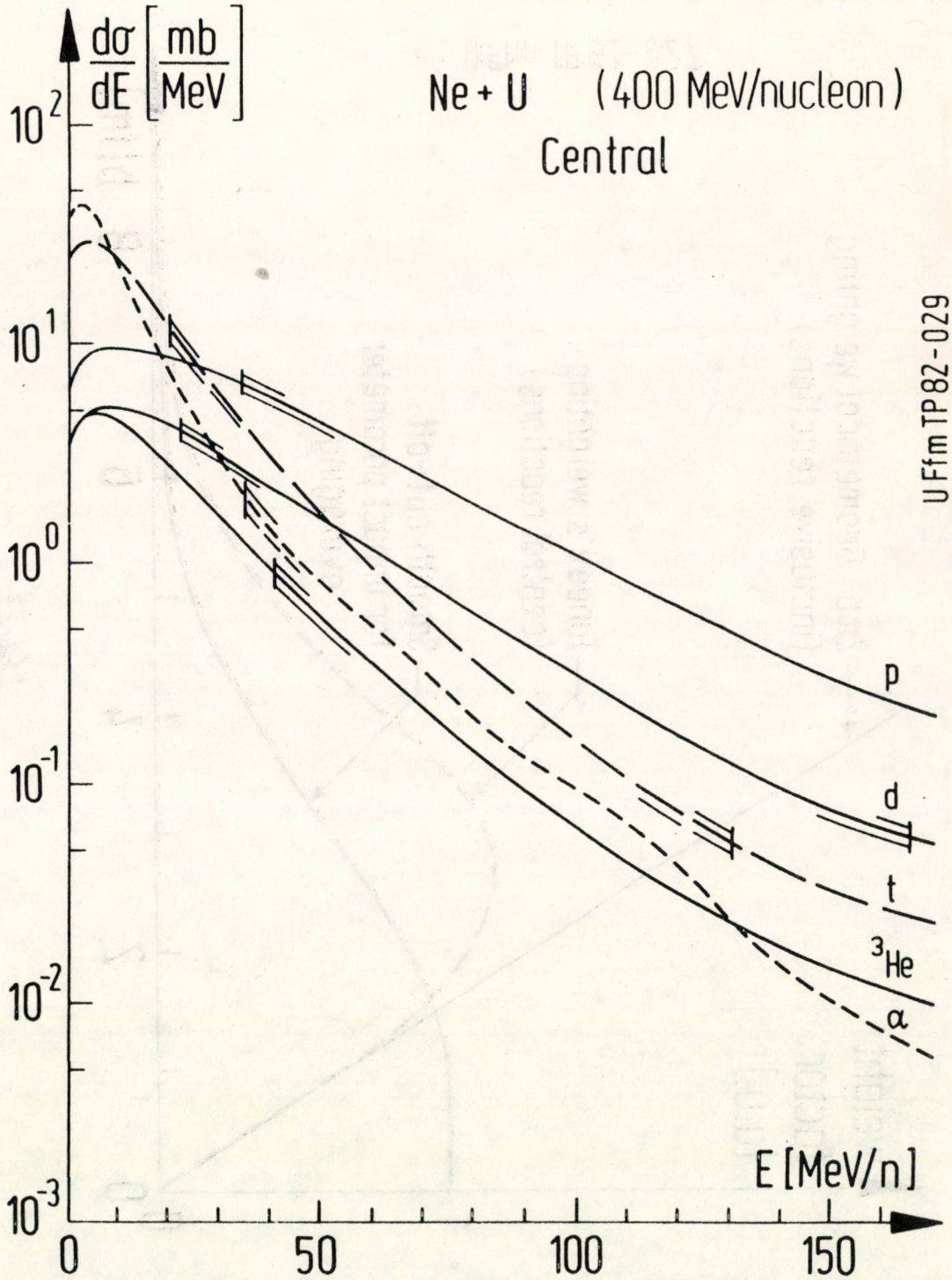
dσ/dE [mb/MeV]
Ne + U (400 MeV/nucleon)
Central
UFfm TP82-029
p
d
t
3He
α
E [MeV/n]
10^2
10^1
10^0
10^-1
10^-2
10^-3
0
50
100
150

Fig. 4

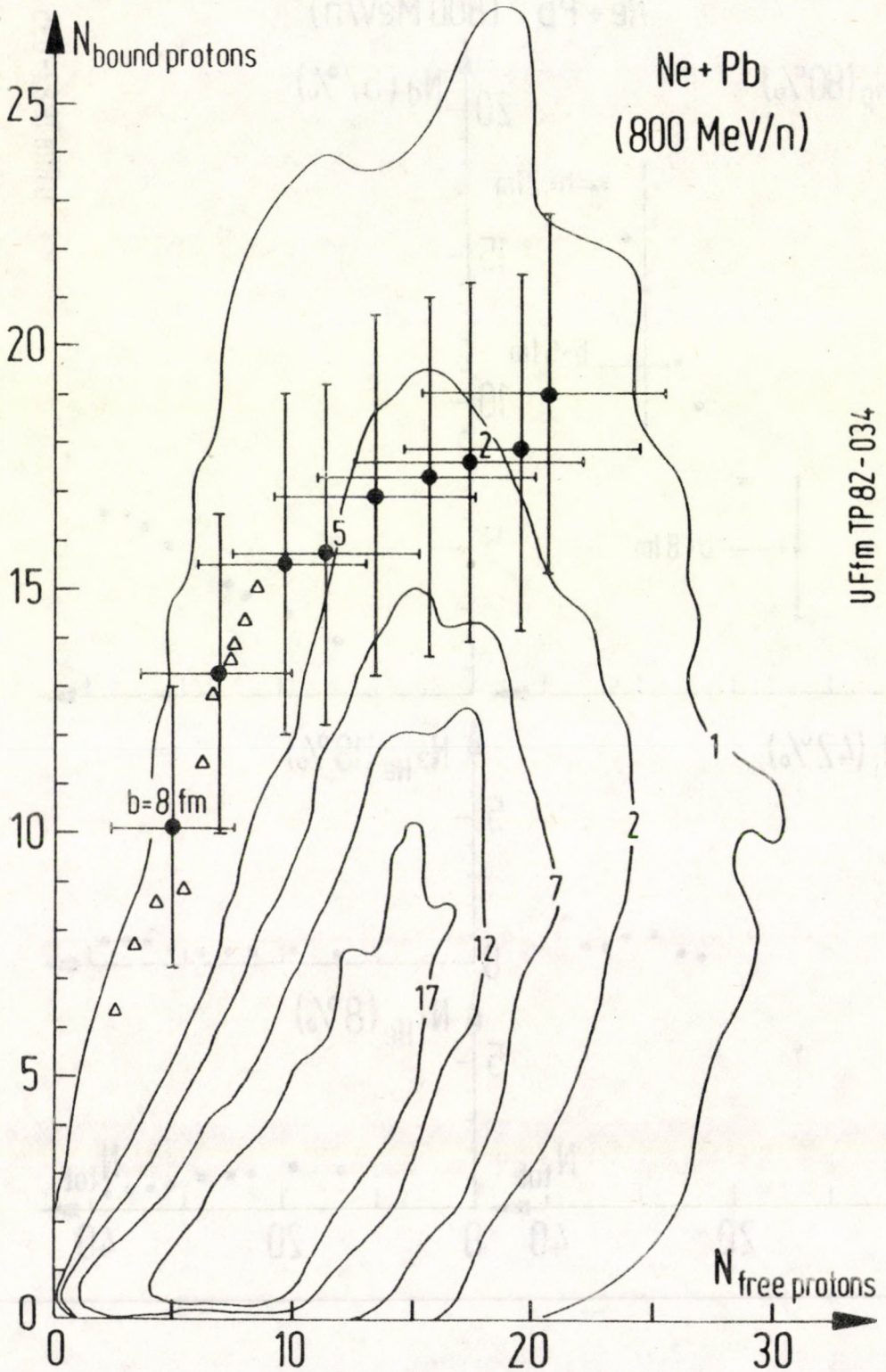
N bound protons
Ne + Pb
(800 MeV/n)
UFfm TP 82-034
b=8 fm
1
2
5
7
12
17
N free protons
0
5
10
15
20
25
0
10
20
30

Fig. 5

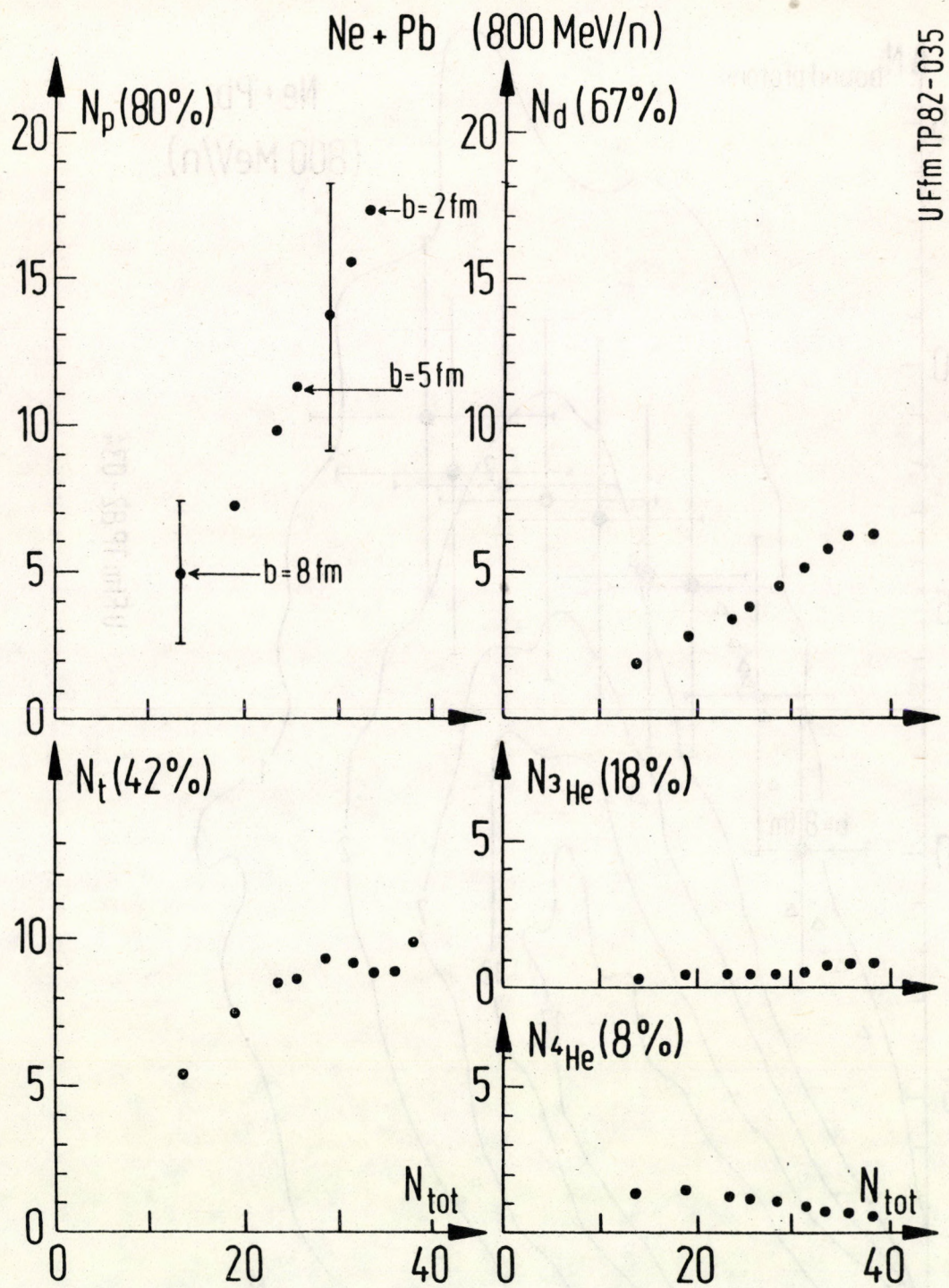
Ne + Pb (800 MeV/n)
Np(80%)
Nd(67%)
Nt(42%)
N3He(18%)
N4He(8%)
b=2fm
b=5fm
b=8fm
Ntot
UFfm TP82-035

Fig. 6

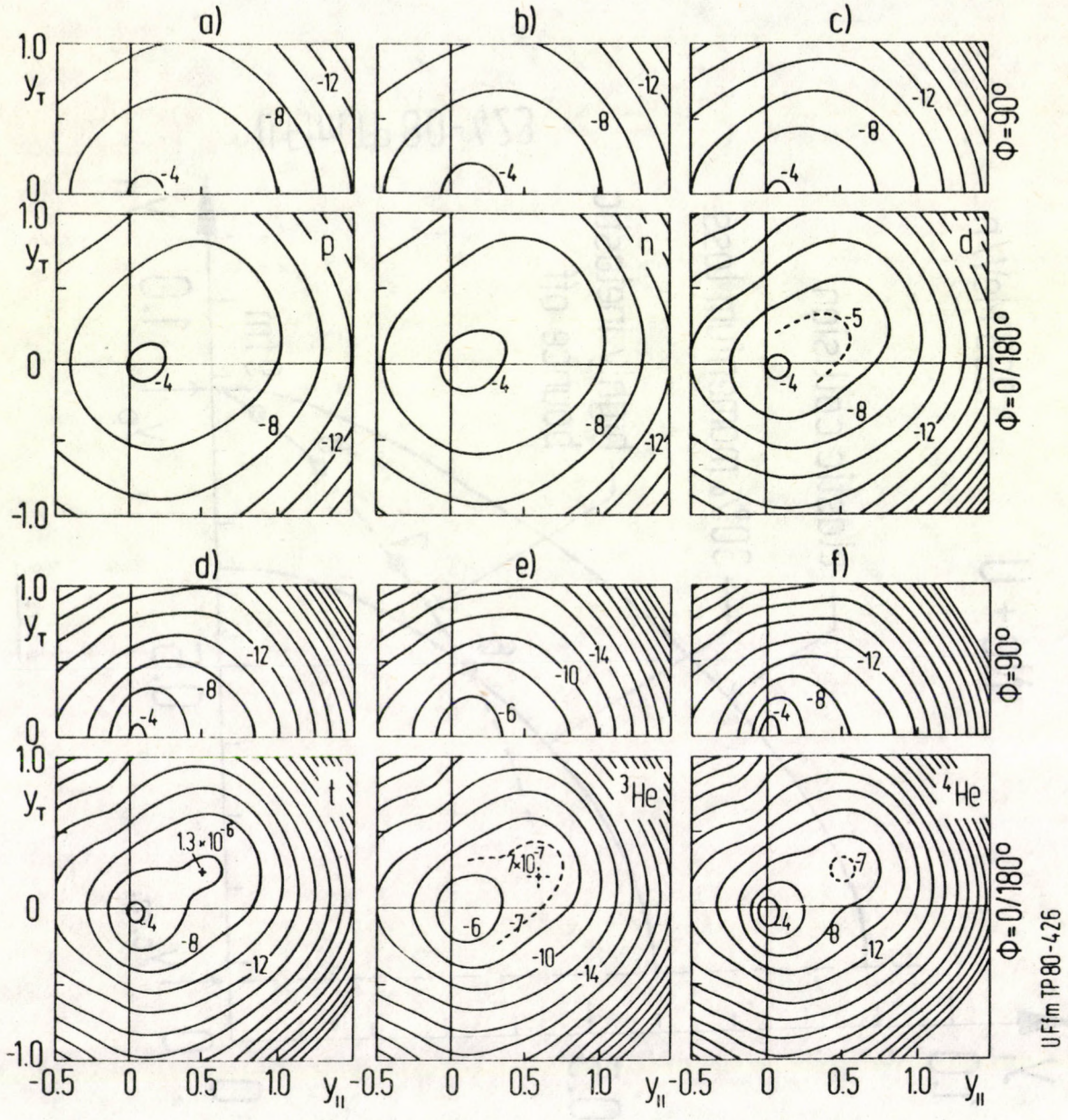
a)
b)
c)
d)
e)
f)
p
n
d
t
3He
4He
Φ=90°
Φ=0/180°
1.0
0
-1.0
y_T
$y_{||}$
-0.5
0.5
1.0
1.3×10⁻⁶
UFfm TP80-426

Fig. 7

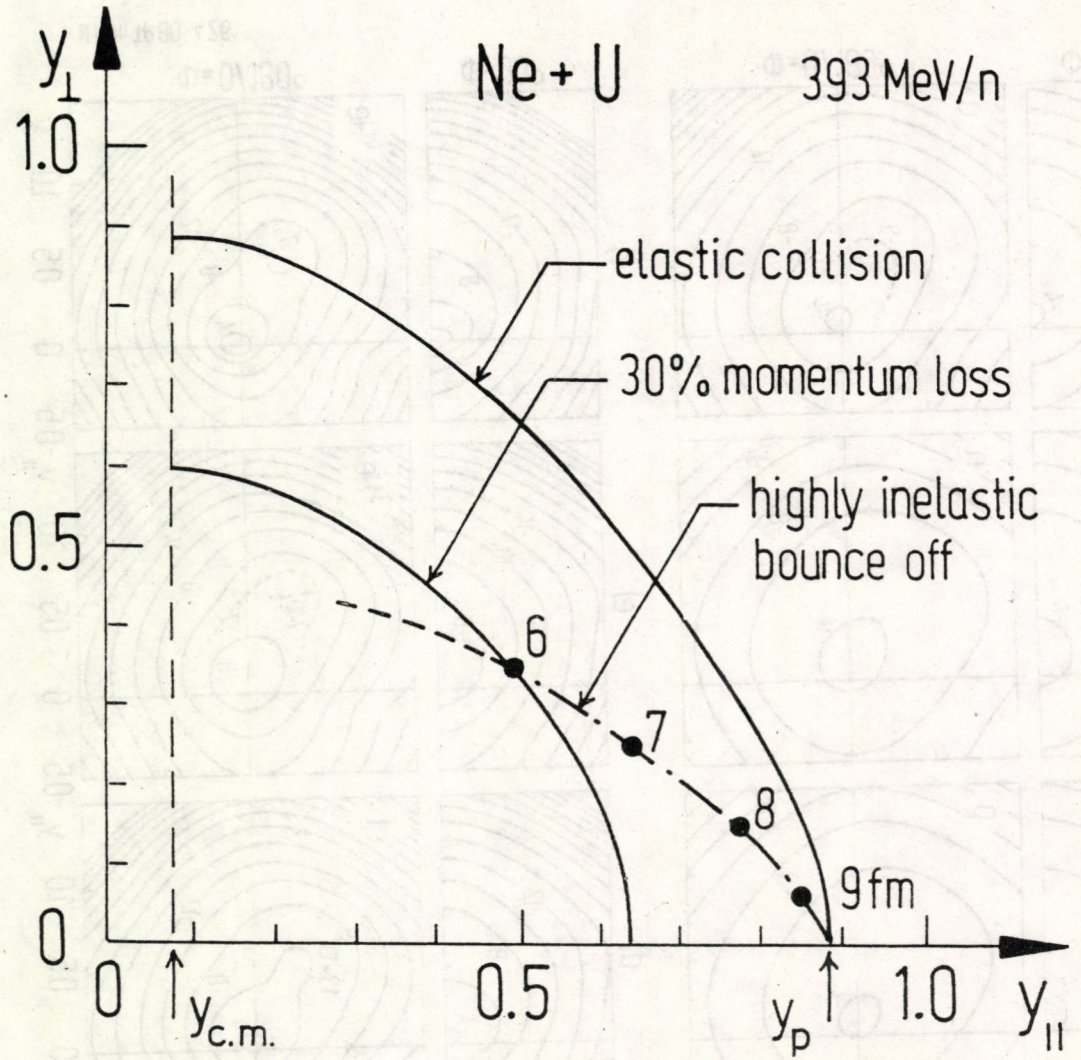
Ne + U
393 MeV/n
$y_\perp$
1.0
0.5
0
elastic collision
30% momentum loss
highly inelastic
bounce off
6
7
8
9fm
0
$y_{c.m.}$
0.5
y_p
1.0
$y_{||}$
UFfm TP 80-423

Fig. 8

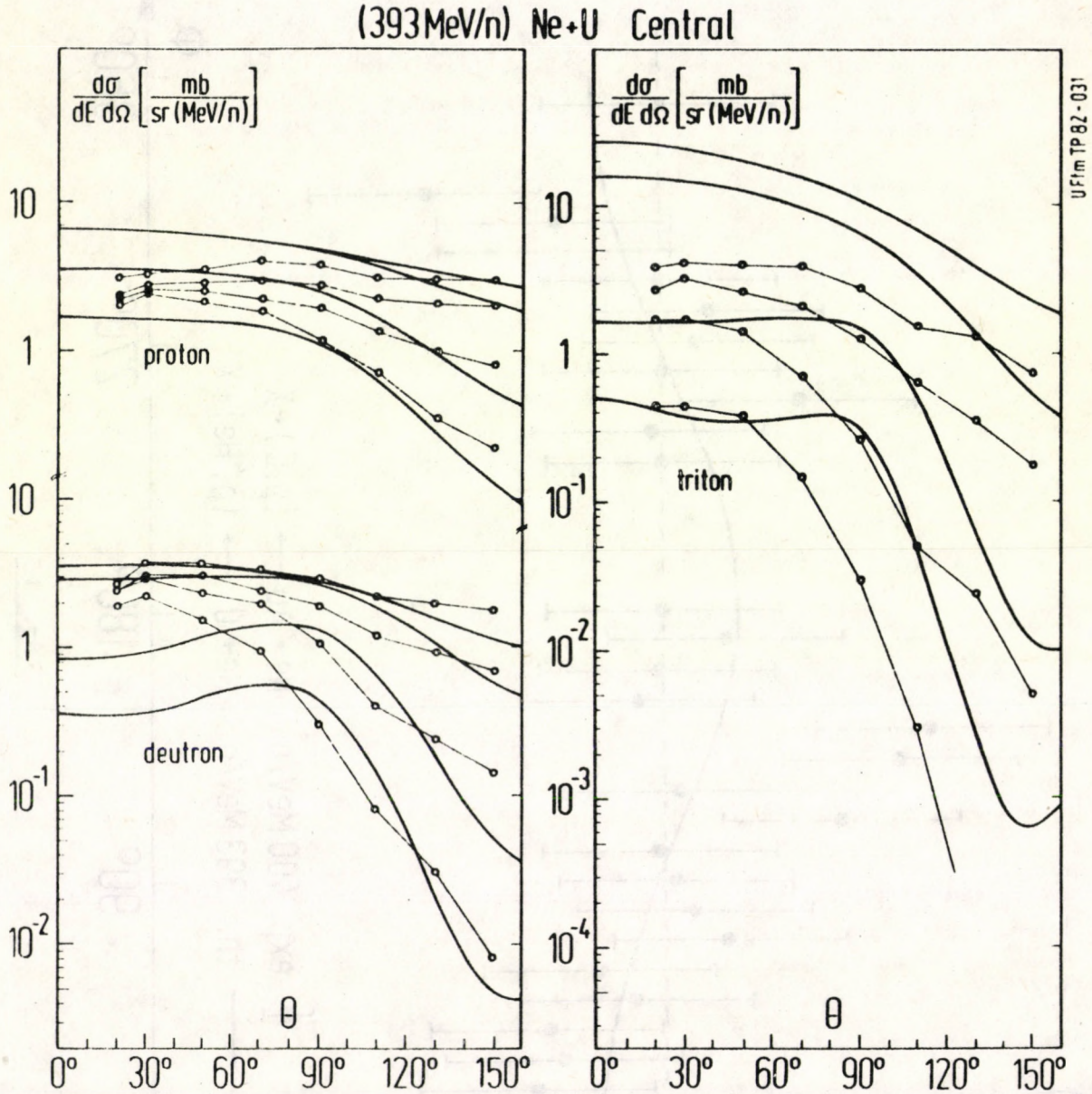
(393MeV/n) Ne+U Central
dσ/dE dΩ [mb/sr(MeV/n)]
proton
deutron
triton
θ
0° 30° 60° 90° 120° 150°
10
1
10
1
10⁻¹
10⁻²
10⁻¹
10⁻²
10⁻³
10⁻⁴
UFtm TP82-031

Fig. 9

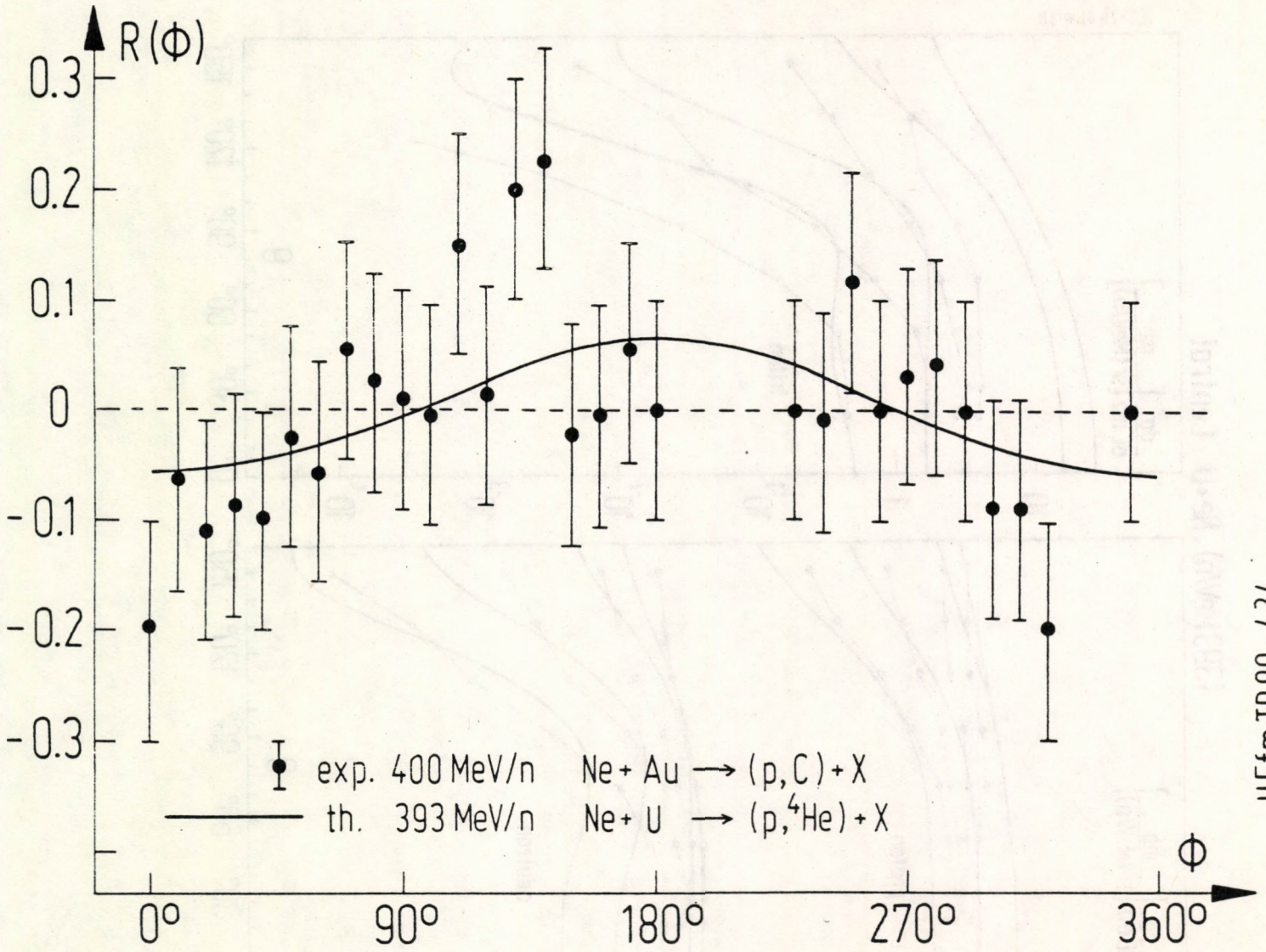

UFfm TP80-424

Fig. 10

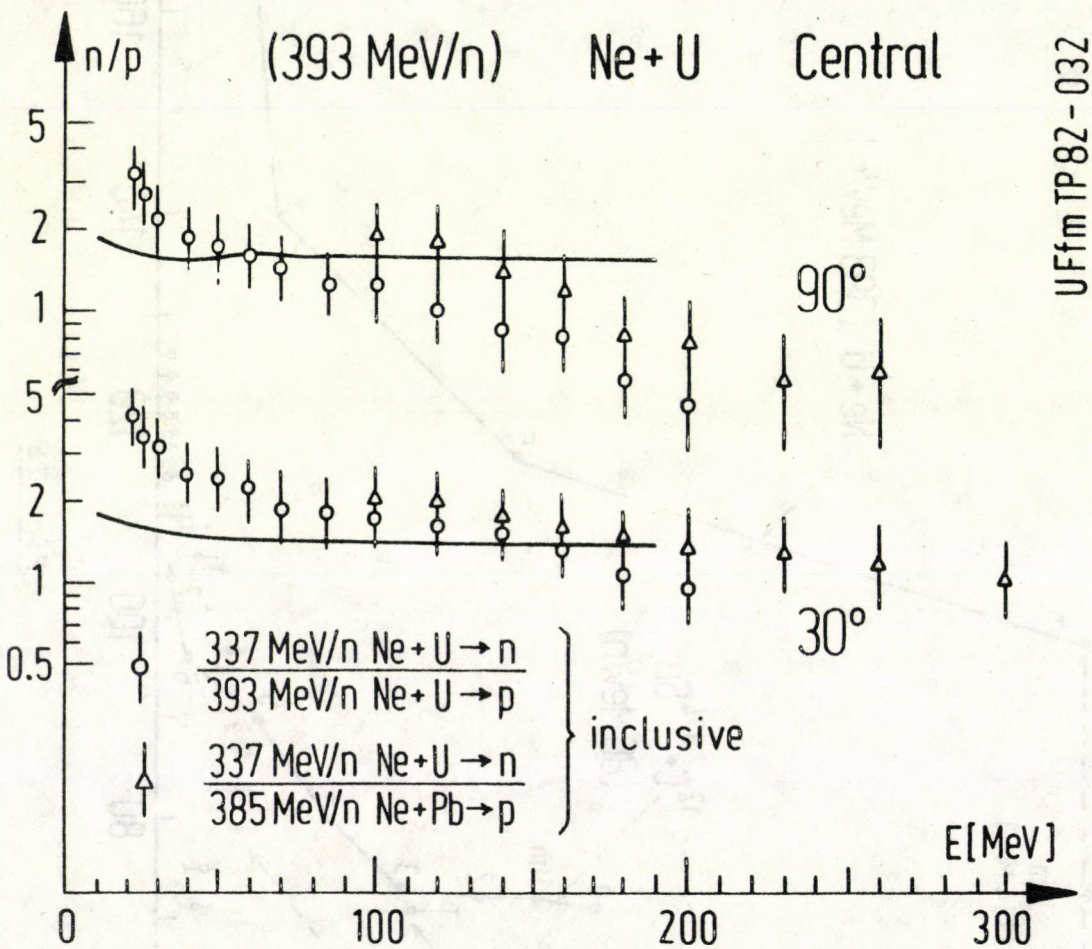
n/p
(393 MeV/n)
Ne + U
Central
UFfm TP 82-032
5
2
1
5
2
1
0.5
90°
30°
337 MeV/n Ne + U → n
393 MeV/n Ne + U → p
337 MeV/n Ne + U → n
385 MeV/n Ne + Pb → p
inclusive
E[MeV]
0
100
200
300

Fig. 11

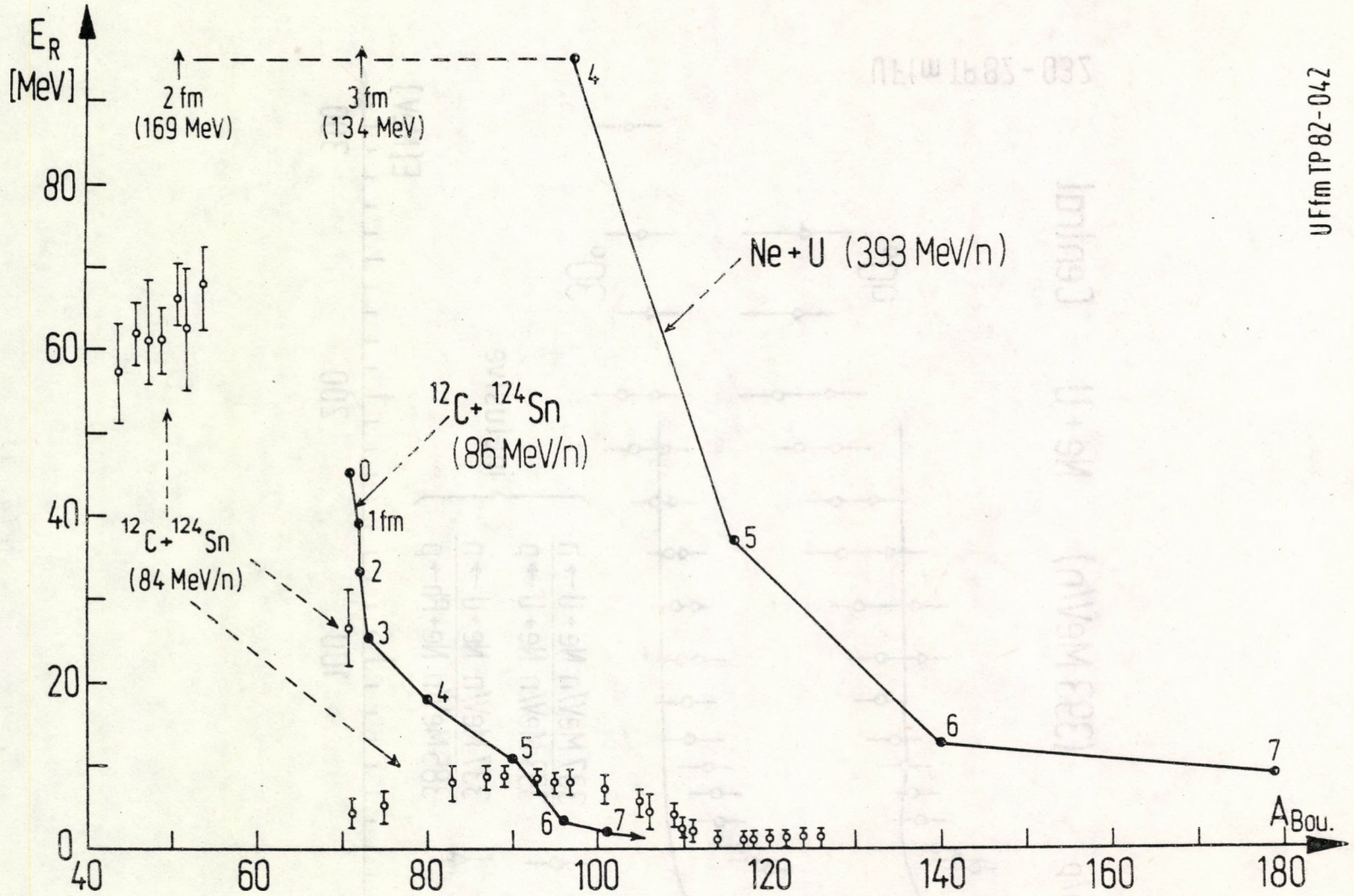
E_R
[MeV]
2 fm
(169 MeV)
3 fm
(134 MeV)
Ne + U (393 MeV/n)
12C + 124Sn
(86 MeV/n)
12C + 124Sn
(84 MeV/n)
1 fm
A_Bou.
0
20
40
60
80
40
60
80
100
120
140
160
180

Fig. 12

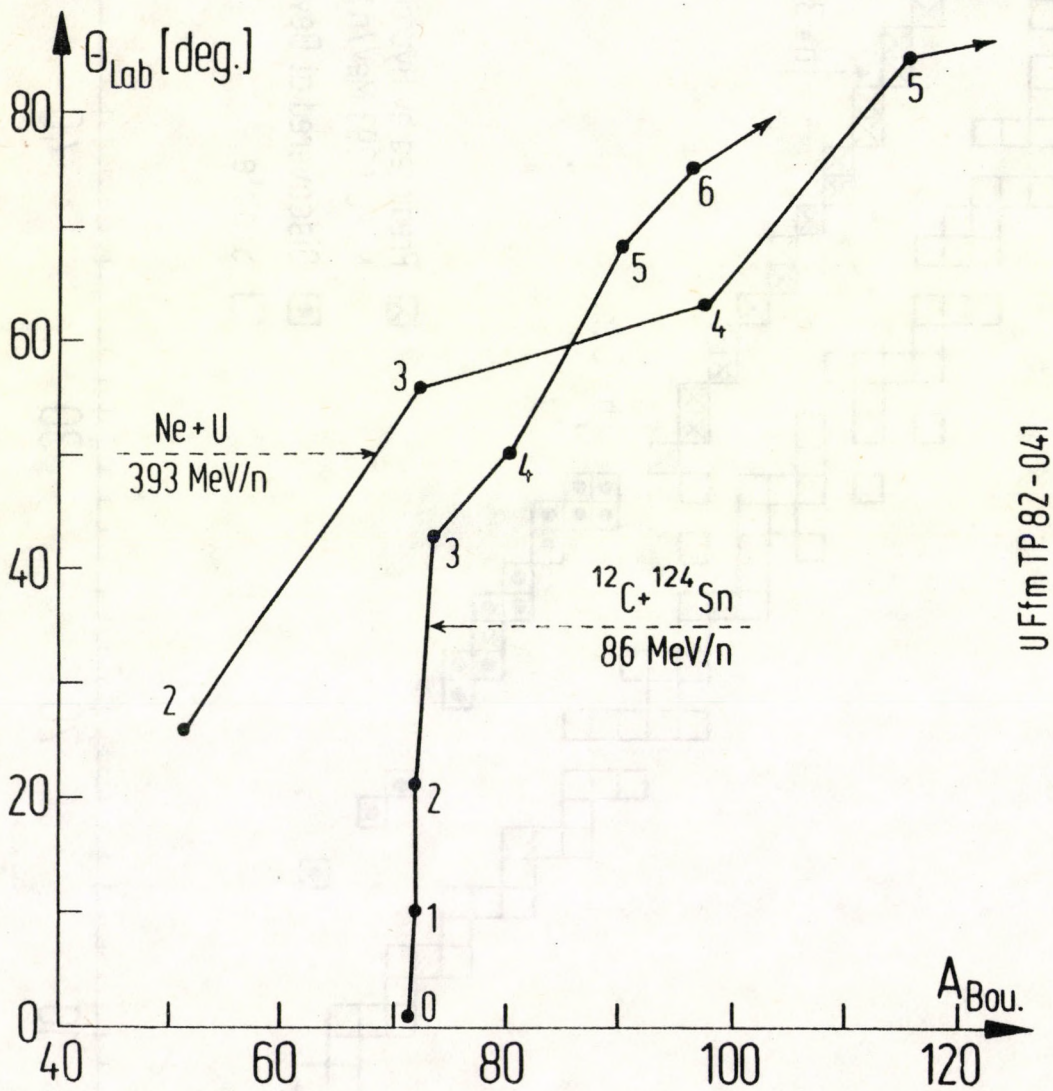
Θ_{Lab} [deg.]
80
60
40
20
0
40
60
80
100
120
$A_{Bou.}$
Ne + U
393 MeV/n
$^{12}C + ^{124}Sn$
86 MeV/n
UFfm TP 82-041
0
1
2
3
4
5
6
2
3
4
5

Fig. 13

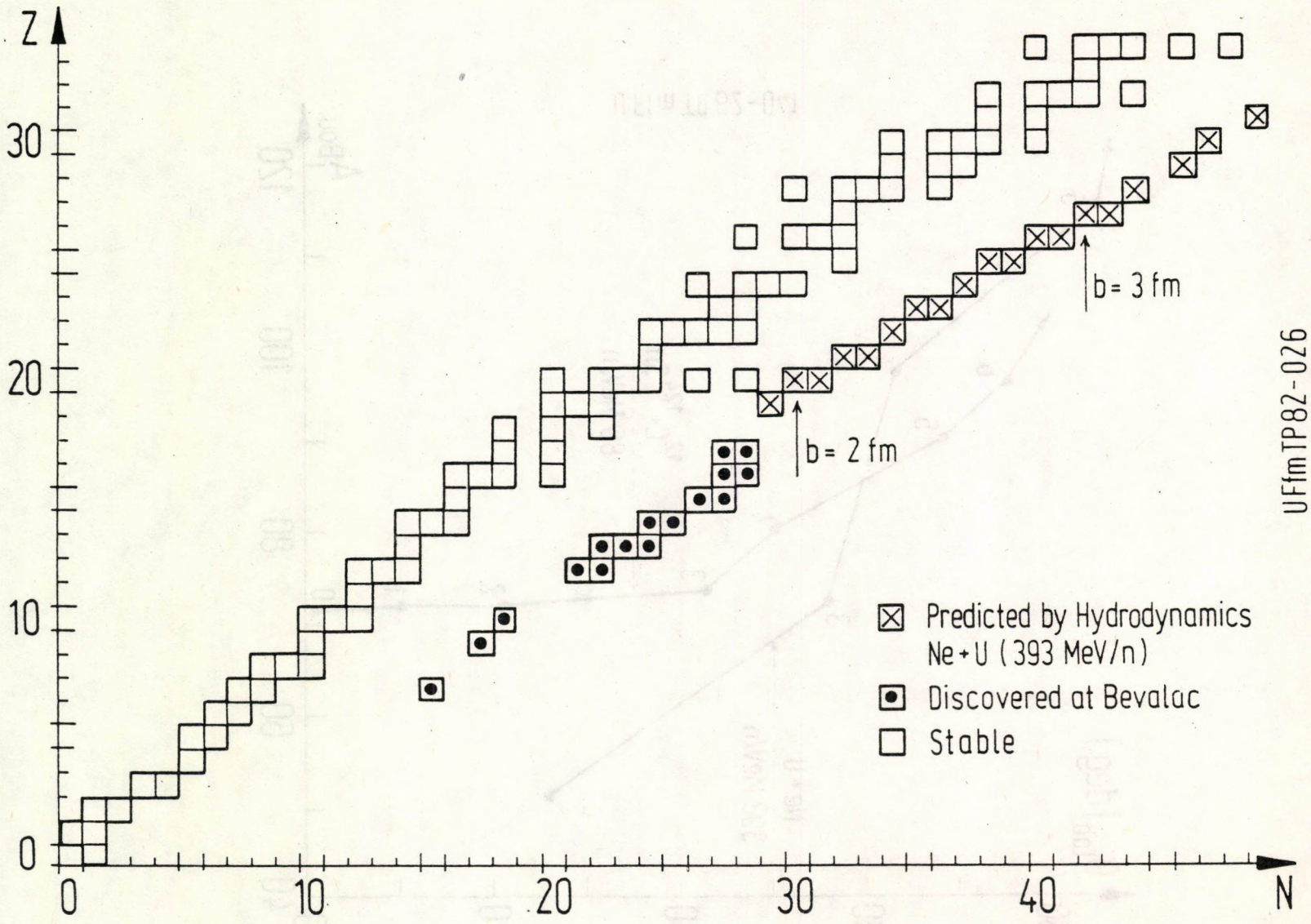
Z
30
20
10
0
0
10
20
30
40
N
b = 3 fm
b = 2 fm
Predicted by Hydrodynamics
Ne + U (393 MeV/n)
Discovered at Bevalac
Stable
UFfmTP82-026

Fig. 14

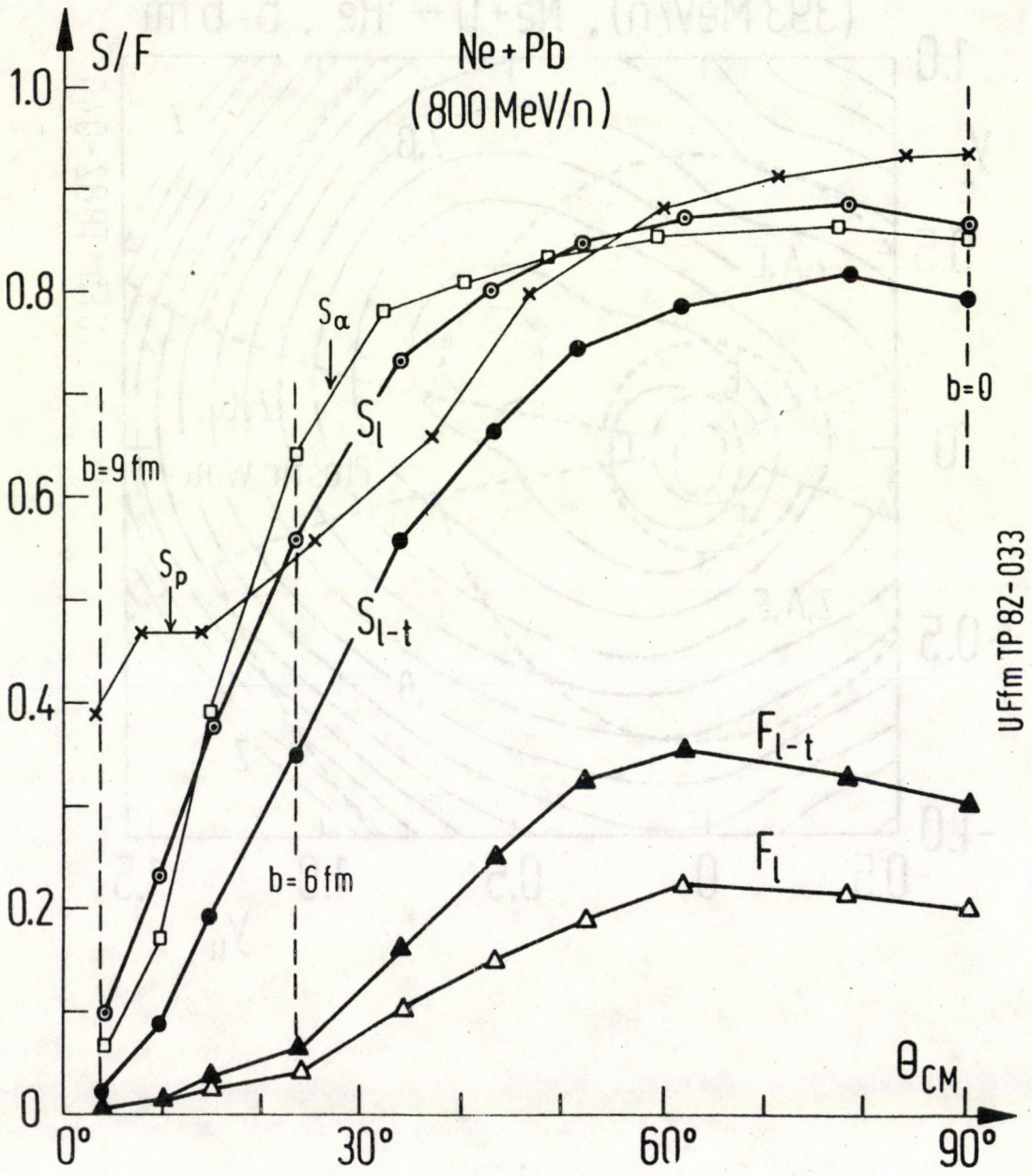
S/F
Ne + Pb
(800 MeV/n)
1.0
0.8
0.6
0.4
0.2
0
S_α
S_l
S_p
S_{l-t}
b=9 fm
b=6 fm
b=0
F_{l-t}
F_l
θ_{CM}
0°
30°
60°
90°
UFfm TP 82-033

Fig. 15

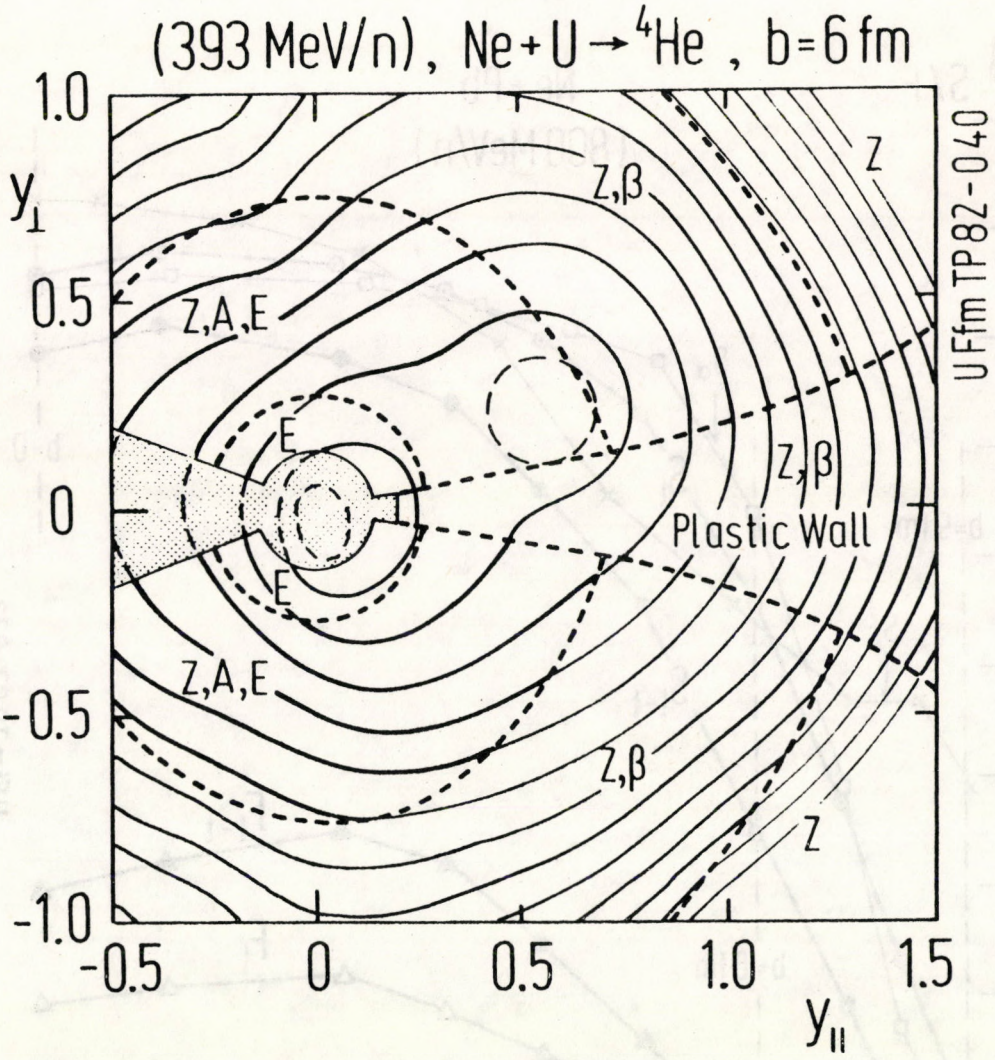
(393 MeV/n), Ne+U → ⁴He , b=6 fm
1.0
0.5
0
-0.5
-1.0
$y_\perp$
-0.5
0
0.5
1.0
1.5
y_{II}
Z
Z,β
Z,A,E
E
E
Z,β
Plastic Wall
Z,A,E
Z,β
Z
UFfm TP82-040

Fig. 16

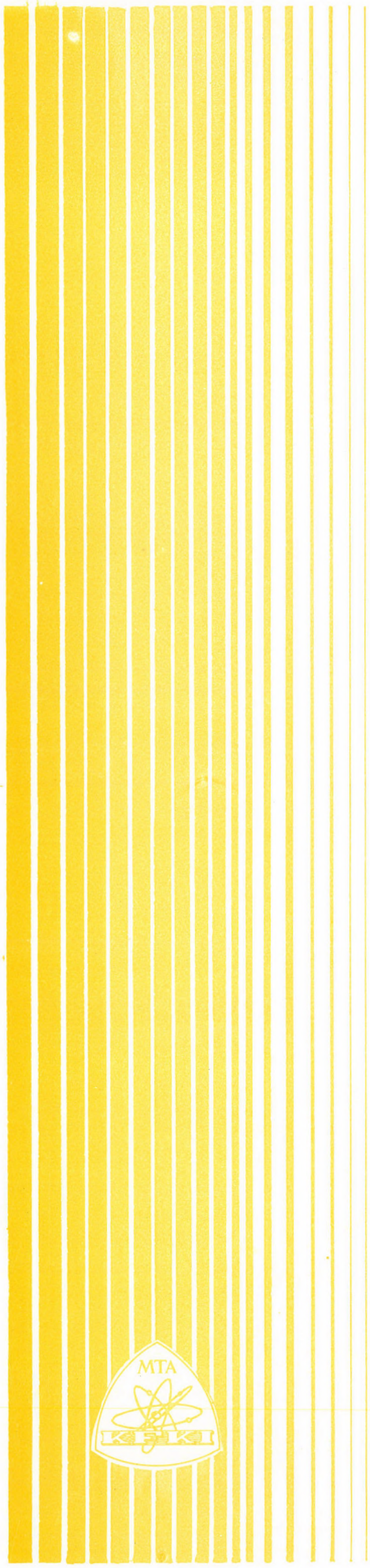

Kiadja a Központi Fizikai Kutató Intézet
Felelős kiadó: Szegő Károly
Szakmai lektor: Zimányi József
Nyelvi lektor: Lovas István
Példányszám: 510 Törzsszám: 82-244
Készült a KFKI sokszorosító üzemében
Felelős vezető: Nagy Károly
Budapest, 1982. május hó